Mineralogy and Petrology
https://doi.org/10.1007/s00710-022-00792-0

ORIGINAL PAPER

La Queglia carbonatitic melnöite: a notable example of an ultra-alkaline rock variant in Italy

Giada Vichi[1] · Maria Grazia Perna[1,2] · Francesco Ambrosio[1] · Gianluigi Rosatelli[1,2] · Daniele Cirillo[1,3] · Sam Broom-Fendley[4] · Nikolay V. Vladykin[5] · Daria Zaccaria[1,2] · Francesco Stoppa[1,2]

Received: 21 December 2021 / Accepted: 4 August 2022

Abstract

Very primitive ultramafic igneous rocks occur at Mt. La Queglia (Abruzzo, Italy). They form a strongly deformed sill–dyke system now tilted vertically. These rocks were initially classified as alnöite and, subsequently, have been suggested to be a carbonatitic olivine melilitite. However, further investigation and interpretation of these rocks is needed due to the presence of hand-specimen-scale textural variation suggesting a complex petrogenesis. We study the texture, mineral chemistry, and whole-rock geochemistry to define three main rock-types. (1) A brecciated rock with an ocellar texture composed of calcite pseudomorphs after olivine and melilite, plus fresh diopside in a groundmass of mica, aegirine, garnet, calcite, apatite, perovskite, titanate and chlorite. Zoned ocelli in this rock show an amoeboid shape, agglutination, and menisci typical of a plastic state. (2) A quenched rock showing a spinifex texture containing long feathery phenocrysts of cpx and mica suspended in a groundmass of nepheline, aegirine, apatite, Ti–rich magnetite, plus abundant calcite and some K-feldspar and zeolites. (3) A coarse-grained rock is composed of calcite plus intergranular glauconite, a mixture of spinel mineral group and Ti–rich magnetite, accessory barite, pyrite, and chabazite-K. The igneous rocks at Mt. La Queglia show extreme SiO_2-undersaturation (33.5–37.3 wt% SiO_2), high MgO contents and TiO_2/Al_2O_3 ratios. Rock-type 1 has a lower Mg number $Mg\# = 100 \times [Mg/(Mg + Fe^{2+})]$, higher Ca number $Ca\# = 100 \times [Ca/(Ca + Mg)]$, high Cr (up to 720 ppm) Ni (up to 379 ppm), higher rare earth elements (REE) contents as well as La/Lu ratio, compared to rock-type 2. Perovskite and chromite accumulation seems an important agent during rock differentiation. Rock-type 3 shows REE cross-over with rock-type 2 suggesting light (L)REE concentration in a carbothermal residuum. Mt. La Queglia rocks are an end-member compared to other Upper Cretaceous and Paleogene Italian lamprophyres, suggesting a low degree of melting of a HIMU (a colloquialism for "high-μ"; referring to mantle domains with high $^{238}U/^{204}Pb$) garnet-bearing mantle source.

Keywords Ultramafic lamprophyres · Melnöites · Carbonatites · Silicate-carbonate phase reaction · HIMU source · La Queglia Mt. · Abruzzo - Italy

Introduction

Genetic relationships between ultramafic and carbonatitic lamprophyres are documented in several large-scale intracontinental rifted areas. Examples include Chuktukon, Russia (Doroshkevich et al. 2019); Maymecha–Kotuy, Russia (Kogarko et al. 2012); Alnö, Sweden (Vuorinen et al. 2005); Gardar, South Greenland (Coulson et al. 2003; Upton et al. 2003; Tappe et al. 2006); Bohemian Massif, Czech Republic (Ulrycht et al. 2014); Laiwu-Zibo, China (Goto et al. 2004) and many others. Most of the information about this rock suite derives from the study of Palaeozoic eroded plutonic complexes. The classification of these ultramafic lamprophyres is challenging. The rocks are generally chemically inextricable but share different mineral associations (polymorphism), based on the presence/absence of olivine plus melilite, the feldspar to feldspathoid ratio, the composition of clinopyroxene and mica, and the amount of carbonate (e.g., Rock 1986). Despite their exotic character and puzzling classification, the study

Editorial handling: P. J. Downes

Author is deceased (formerly Vinogradov Institute of Geochemistry, SBRAS, 1a Favorsky St., Irkutsk, Russia, 664033)

✉ Gianluigi Rosatelli
grosatelli@unich.it

Extended author information available on the last page of the article

of these rocks is of paramount importance because they provide information about the composition of the upper mantle and its processes.

Carbonatitic activity associated with lamprophyres is well documented in Italy and can be traced back to the Lower Cretaceous (Vichi et al. 2005). A Palaeocene (62–58 Ma) lamprophyre cycle is known from the NE margin of the Adria domain, which is a part of the African continental plate (*e.g.*, Stoppa et al. 2014). The Mt. La Queglia rocks, which were emplaced during the Ypresian (54 Ma), belong to this cycle.

Mt. La Queglia rocks were first described as serpentinite after peridotite (Bellini 1957) but were subsequently reclassified as an ultramafic lamprophyre with alnöitic affinity (Barbieri and Ferrini 1984; Durazzo et al. 1984). Based on the modal abundance of melilite and the paucity of hydroxyl-bearing minerals, Vichi et al. (2005) suggested classifying these rocks as olivine melilitite according to the International Union of Geological Sciences (IUGS) recommendations (Le Maitre 2002). This paper encompasses updated criteria to clarify the nature of these rocks, and describe their source composition, magma genesis, and petrogenesis.

Local geology

Mt. La Queglia is on the eastern side of the Gran Sasso – Morrone massif (Fig. 1a). It consists of a N–S asymmetric anticline thrust eastward over Messinian and Plio-Pleistocene foredeep deposits (Bigi et al. 1995; Brozzetti et al. 2020; Cirillo et al. 2022). The stratigraphic sequence of Mt. La Queglia consists of Upper Cretaceous – Eocene pelagic limestones and Eocene—Miocene bioclastic limestones – (from bottom to top).

The western side of the Mt. La Queglia anticline is characterised by a segmented, sub-vertical, N–S high-angle fault, variously interpreted as an extensional fault, active during the Miocene (Bigi et al. 1995; Scisciani et al. 2000), or as a Pliocene back-thrust (Ghisetti and Vezzani 1991) located within the extensional seismogenic province of Italy (*sensu* Lavecchia et al. 2021, 2022). Alternatively, being not tilted or deformed, the faulting may be Pleistocene in age.

The igneous body crops out at the western side of Mt. La Queglia and intrudes the lower portion of Upper Cretaceous-Eocene limestones (Figs. 1b, c, d and e). It was emplaced under extensional tectonic conditions and then folded during the Pliocene. The igneous body seems roughly parallel and adjacent to the fault. However, evidence of the crosscutting relationship between the fault and the igneous rocks suggests the latter are older. Mt. La Queglia igneous rocks have a mica Ar/Ar age of ~ 54 Ma (Laurenzi M., personal communication). Eocene magmatism manifested at Mt. La Queglia, Punta delle Pietre Nere, and borehole samples (surveys Maiella 1) suggesting a regional igneous phase. Elongate, irregularly shaped igneous bodies discontinuously crop out on the western side of the Mt. La Queglia anticline. They form an intricate *en-echelon* body up to 7 m in thickness and about 60 m in length. Most of the exposed contacts with the limestone country rocks are tectonised with polished, striated surfaces. Thermometamorphic contact phenomena are not apparent in the field. There is no sign of plastic deformation of the encasing rocks or assimilation. Igneous rocks are semi-concordant with sedimentary layering and are generally sub-vertical. Low-angle inclinations are possibly related to oblique dykes originally interconnecting sills at a small scale. Pervasive boudinage-foliation and grain flow are seen where the thickness of the igneous body is reduced to less than 1 m. Minor fault planes, parallel to the main one, dissect the igneous rocks or mark the contact between the country rocks and different rock facies. Bigi and di Bucci (1987) mapped isolated outcrops further to the north, but the field survey does not confirm this data.

Two main magmatic rock types have been recognised in the field and extensively sampled (Fig. 1c). The igneous rocks are brecciated with rotated clasts (Fig. 2a and b) wrapped by sparry cement and pervaded by carbonate veins (Fig. 2c and d). There are country rock clasts included in the rock with sign of alteration and thiny recrystallised reaction rims. Ocellar structures are widespread and migrate from the centre of the dikes towards the contact zone with host rock and can reach up to 0.5 cm in diameter (Fig. 2e).

Rock-type 1 forms the main igneous body (Fig. 1c). It is dark grey to greenish-reddish, porphyritic with an aphanitic groundmass (Fig. 2e). Sparry-calcite veins and dark green amygdales are also present. Rock-type 2 is a fine-grained spinifex-textured rock (Fig. 2f) mainly located in the south-eastern part of the outcrop (Fig. 1c). In addition, a third common rock-type is a white and green, coarse-grained calcitic rock occurring at the contact with the host-rock and forming sparse lenses in the igneous rock (Fig. 2g).

Methods

A drone was used to capture images of hard-to-access parts of Mt. La Queglia in order to produce a high-resolution outcrop model able to distinguish the different rock types and therefore aid mapping (Westoby et al. 2012; James and Robson 2012; Bemis et al. 2014; Cirillo 2020; Bello et al. 2021, 2022). The instrumentations used were a base (Emlid Reach RS2 GNSS/RTK L1,L2,L5 system), positioned on the ground, and an antenna rover (L1/L2 RTK/PPK) mounted above the drone (DJI Mavic 2 Pro) that records raw global navigation satellite system (GNSS) logs which were then processed to obtain accurate positioning of the pre-established flight path (Cirillo

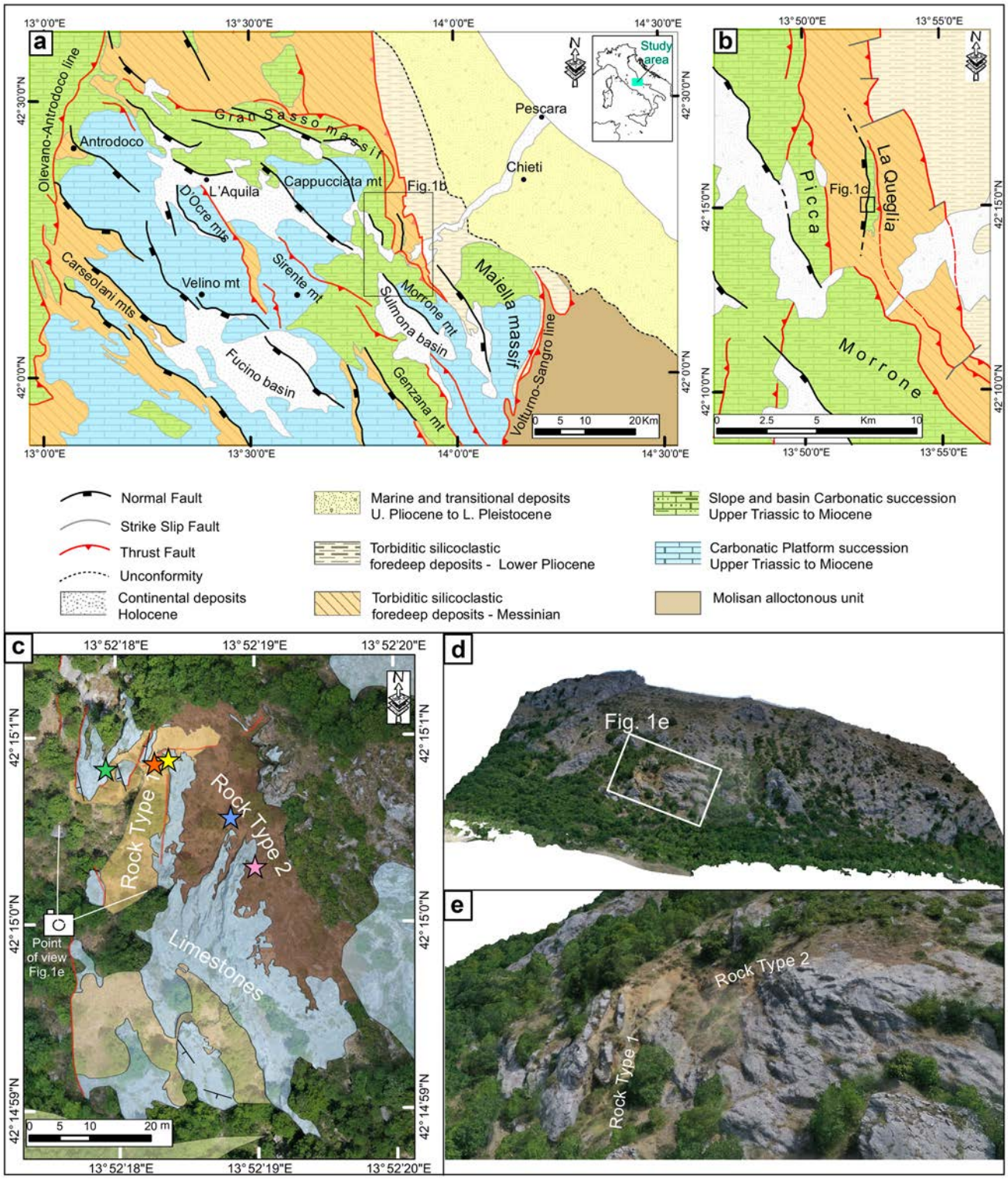

Fig. 1 **a** General sketch map of the Abruzzo Apennines. **b** Detail of the Mt. La Queglia structural setting. **c**, **d** and **e** Remote sensing elaboration of ultramafic rocks of Mt. La Queglia and rock-type distribution. The stars represent the sampling points: orange star: rock-type 1 facies a; yellow star: rock-type 1 facies b; pink star: rock-type 2 facies c; purple star: rock-type 2 facies d; green star: rock-type 3

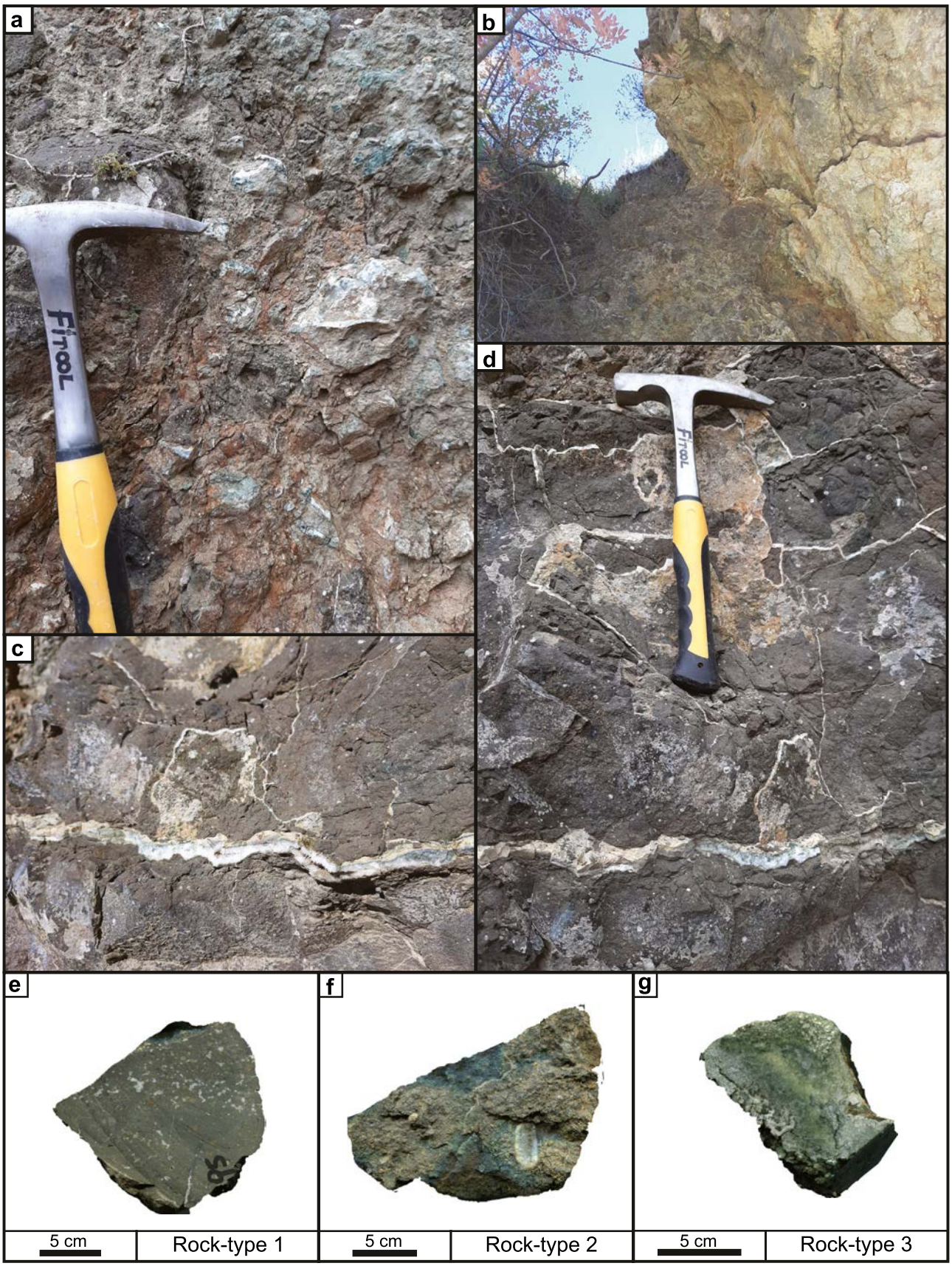
a
b
c
d
e
f
g
5 cm
Rock-type 1
5 cm
Rock-type 2
5 cm
Rock-type 3

◂**Fig. 2** **a** Brecciated rock-type 1 without ocelli. **b** Breccia-dike at contact with sedimentary host rock. **c** and **d** Ocellar facies pervaded by secondary calcite veins. **e**, **f**, **g** Hand specimens samples of La Queglia Mt. **e** Rock-type 1, **f** Rock-type 2 and **g** Rock-type 3

et al. 2022). A total of 290 photos were acquired, with a minimum front and side overlap of 70%. Photogrammetric processing combines digital surface models (DSM) and digital outcrop models (DOM) with high-resolution imagery and topography. Processing with Agisoft Metashape Professional software was necessary to obtain a high spatial resolution for the DOM. The use of this software led to the following results through Ultra High-Quality processing: 241,850 sparse point clouds, 543,015,433 dense point clouds, meshes and textures, 87,001,171 faces of 3D models, tiled models, digital elevation model (DEM) and an orthomosaic model at 2.23 cm/px.

Bulk-rock analyses for 64 elements, including CO_2 and REE, were determined using multiple methods. Trace elements were analysed by inductively coupled plasma–mass spectrometry (ICP–MS) using an ELEMENT2 instrument (FinniganMAT, Bremen, Germany). Four certified Multi-element solutions (CLMS-1–4, SPEX, USA) were employed for constructing calibration graphs. In preparing these and other solutions we used the water purified through Millipore-ELIX-3 (Miilipore, SA, France) device. The standards used were DNC-1 and BIR-1 (Supplementary Table S1). CO_2 contents were measured using a Dietrich-Frühling calcimeter, with pure calcite used as a standard.

Cold-cathodoluminescence images were obtained using a CITL Mk5 electron source attached to a standard petrographic microscope equipped with a Nikon DS Ri2 camera. The electron beam was typically operated at a voltage of approximately 10 kV and a current of 250 µA. Images were acquired with a 2 s exposure time. Composite images were stitched together using Adobe Photoshop.

Minerals were analysed using a Phenom XL scanning electron microscope (SEM) and, on polished thin sections, using a CAMECA SX50 electron probe micro-analyser (EMPA). Silicate minerals were analysed with a 15 kV and ~ 20 nA beam with 2–15 µm focal-spot diameter, while carbonates were analysed with a 15 kV and 10 nA beam with 10–15 µm spot diameter. X-ray lines analysed and the natural reference or synthetic standard used for calibration were the following: Si-Kα – synthetic wollastonite; Ti-Kα – synthetic TiO_2; Al-Kα – synthetic corundum; Cr-Kα – Cr metal; Fe-Kα – Fe metal; Mn-Kα – Mn metal; Mg-Kα – natural aegirine; Zn-Kα – Zn metal; Ni-Kα – niccolite; Na-Kα – natural jadeite; REE-Lα – phosphates of individual REEs; Sr-Lα – natural celestine or synthetic $SrTiO_3$; Zr-Lα – natural zircon; Nb-Lα – pure Nb metal; Ta-Lα – Ta metal; Th-Mα – synthetic ThO_2; Ba-Lα – synthetic BaF; K-Kα – synthetic KBr; S-Kα – natural pyrite; F-Kα – floorapatite for apatites and natural horneblende for all other minerals analysed; Cl-Kα – natural scapolite. For Ca (Ca- Kα was measured), the calibrant material used for apatites was natural fluorapatite, for calcite either natural calcite or aragonite were used; and for all other minerals synthetic wollastonite was used as reference material. The counting times were 30 s on peak and 10 s on background. The correction procedure applied was Phi-rho-Z correction. Detection limits were estimated for oxides as two times the standard deviation of the background counts (2σ).

X-Ray powder diffraction (XRPD) analysis was performed by means of a Bruker D2 Phaser diffractometer. Cu-Kα radiation was used.

Sr, Nd, and Pb isotopes were analysed using a Finnigan-MAT 261 multi-collector, solid-source mass spectrometer operated in static mode. Standards run during this study yielded the following values: NBS-987 $^{87}Sr/^{86}Sr = 0.71025 \pm 0.00003$, La Jolla $^{143}Nd/^{144}Nd = 0.51187 \pm 0.00003$, NBS-981 $^{206}Pb/^{204}Pb = 16.890 \pm 0.010$, $^{207}Pb/^{204}Pb = 15.429 \pm 0.013$, $^{208}Pb/^{204}Pb = 36.498 \pm 0.042$. The measured Sr and Nd isotopic ratios for all samples were corrected for fractionation to $^{88}Sr/^{86}Sr = 8.3752$ and $^{146}Nd/^{144}Nd = 0.7219$. An average fractionation factor of 0.12 per mass unit was applied to all measured Pb isotope ratios based on repeat analyses of NBS-98 standard.

Results

Petrography and mineral chemistry

Generalities on rock types

Microscopic observations of Mt. La Queglia rocks reveal distinct textural and compositional changes. Abrupt changes in the abundance of olivine and melilite are accompanied by an increase in felsic components and carbonate contents, and a change in rock texture. These changes allow the identification of different facies among the three rock-types. Transitional facies show a patchy composition forming a different, sparsely distributed, mineralogical assemblage with a different chemical composition. The absence of plagioclase, paucity of amphibole and feldspar and the presence of calcite pseudomorphs after melilite, along with perovskite and garnet, suggest that the rocks may be an ultramafic lamprophyre (UML). In the following paragraphs, a detailed description of the various facies follows.

Rock-type 1, facies a (sections Q9, Q19b, Q19-2, Q19d) (Fig. 3a and b): This is a fine-grained rock with a seriate porphyritic texture and an intersertal/intergranular groundmass. Abundant phenocrysts of euhedral olivine are completely replaced by alteration products such as chlorite and calcite. Only 1.2 vol% of fresh olivine is documented by XRPD. Euhedral calcite pseudomorphs

after melilite sometimes preserve a peg-like structure (Stoppa et al. 2003). Euhedral fresh diopside is up to 21 vol%. Diopside–augite, altered olivine and pseudomorphs after melilite are immersed in an intersertal/intergranular groundmass of acicular aegirine–augite associated with carbonate, chromite (6 vol%), biotite (14 vol%), nepheline (11 vol%), garnet, and apatite (6.8 vol%). Perovskite is up to 4 vol% and associated with an unidentified TiO_2

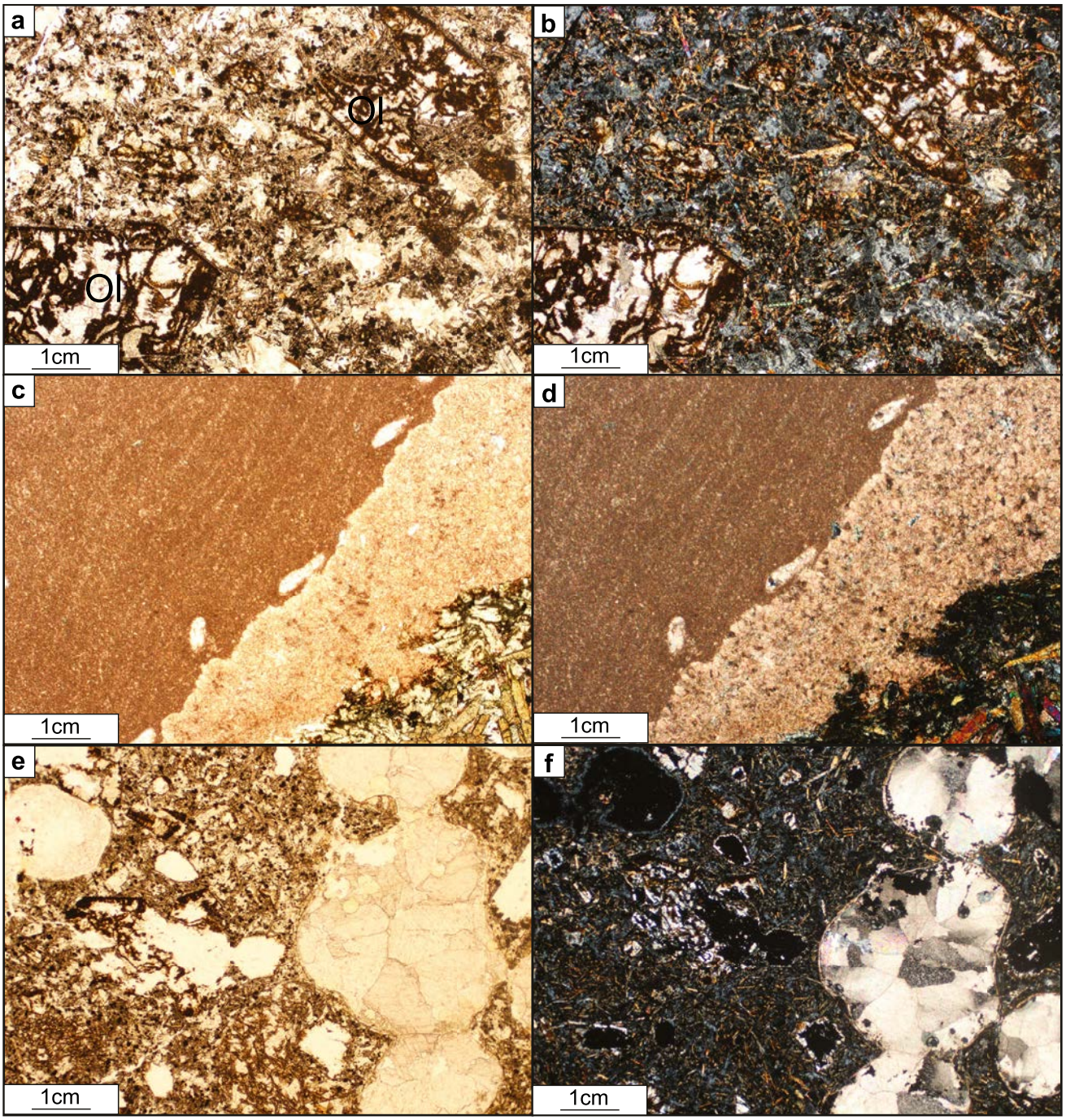

Fig. 3 Plane-polarised (left) and cross-polarised (right) transmitted-light images of Mt. La Queglia rock-type 1, 2 and 3. **a** and **b** Mt. La Queglia rock-type 1, facies a, sample Q19d. Large olivine pseudomorph in calcite in an intergranular-intersertal groundmass with clinopyroxenes, melilite-calcite pseudomorph frame and mesostasis of calcite, foids, chlorite and perovskite. **c** and **d** Detail of a xenolith enveloped in rock-type1 facies a showing a recrystallized rim at the contact with the igneous rock and some ocelli aligned along the inner part of the contact developing in the unaltered micritic sedimentary limestone. **e** and **f** Mt. La Queglia rock-type 1, facies b, sample Q20. Large coalescent ocelli showing mosaic textured calcite pulling apart the groundmass and clinopyroxene prisms

polymorph. The chloritized groundmass is spotted with magnesiochromite. Rare accessory minerals are harmotome, chabazite-Ca and kaolinite. Elongate rounded limestone clasts of a few cm in size show a sharp contact with the igneous rocks marked by a mosaic textured calcite and an unaltered core. A few ocelli occur near the recrystallised rim (Fig. 3c and d).

Rock-type 1, facies b (section Q11, Q5, Q20, Q19a, Q6) (Fig. 3e and f): This is characterised by abundant spherical or drop-like ocelli, which are often coalescent

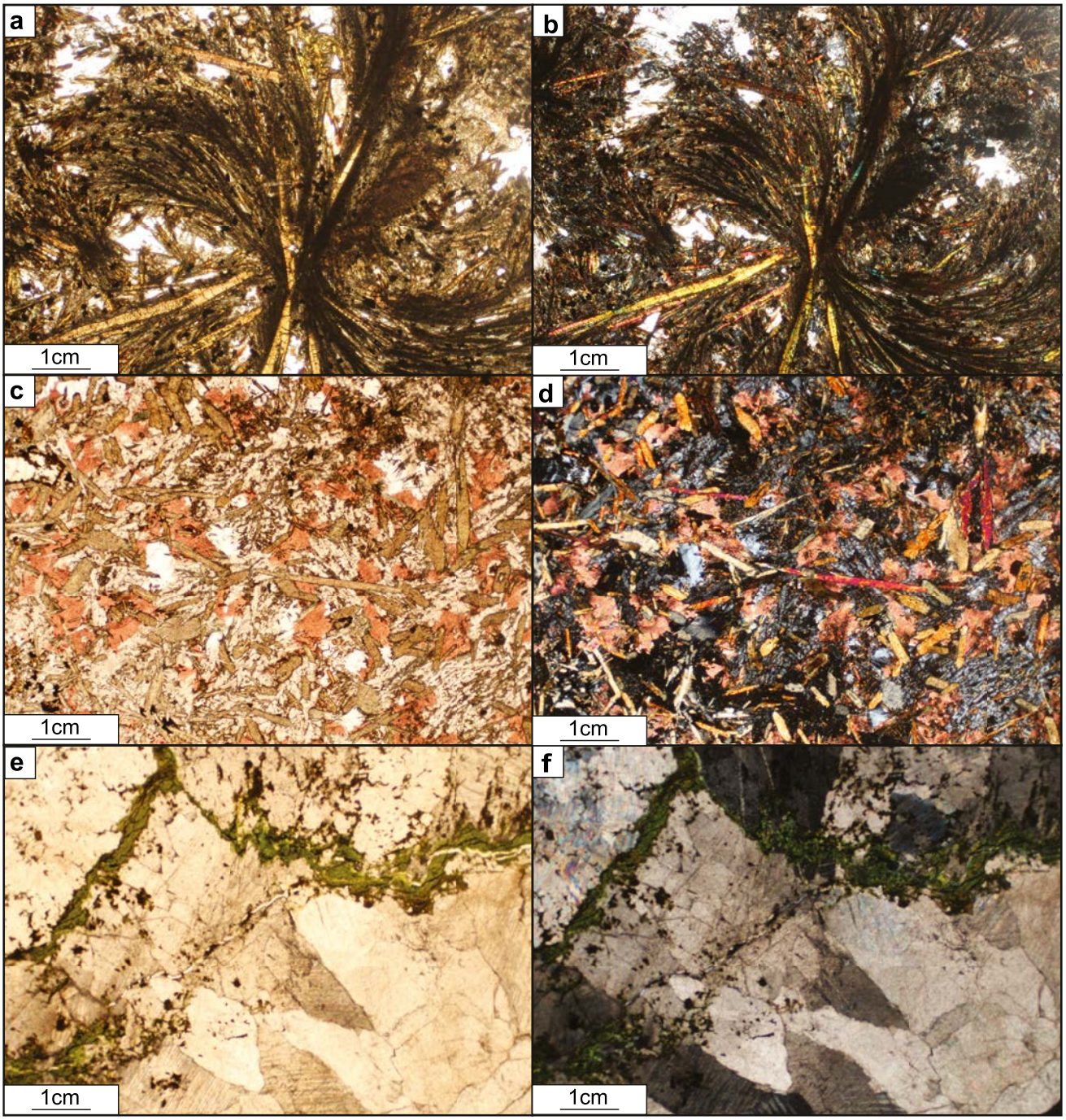

Fig. 4 Plane-polarised (left) and cross-polarised (right) transmitted-light images of Mt. La Queglia rock-type 1, 2 and 3. **a** and **b** Mt. La Queglia rock-type 2, facies c, sample QN1. Large feathered curved branching clinopyroxene and mica in a calcite groundmass. **c** and **d** Mt. La Queglia rock-type 2, facies d, sample VT22/6a. Alizarine stained K-feldspar and carbonate framed by clinopyroxene prims. **e** and **f** Mt. La Queglia rock-type 3, sample QUEGLIA1. Equigranular coarse-grained calcite with intergranular glauconite and spinels

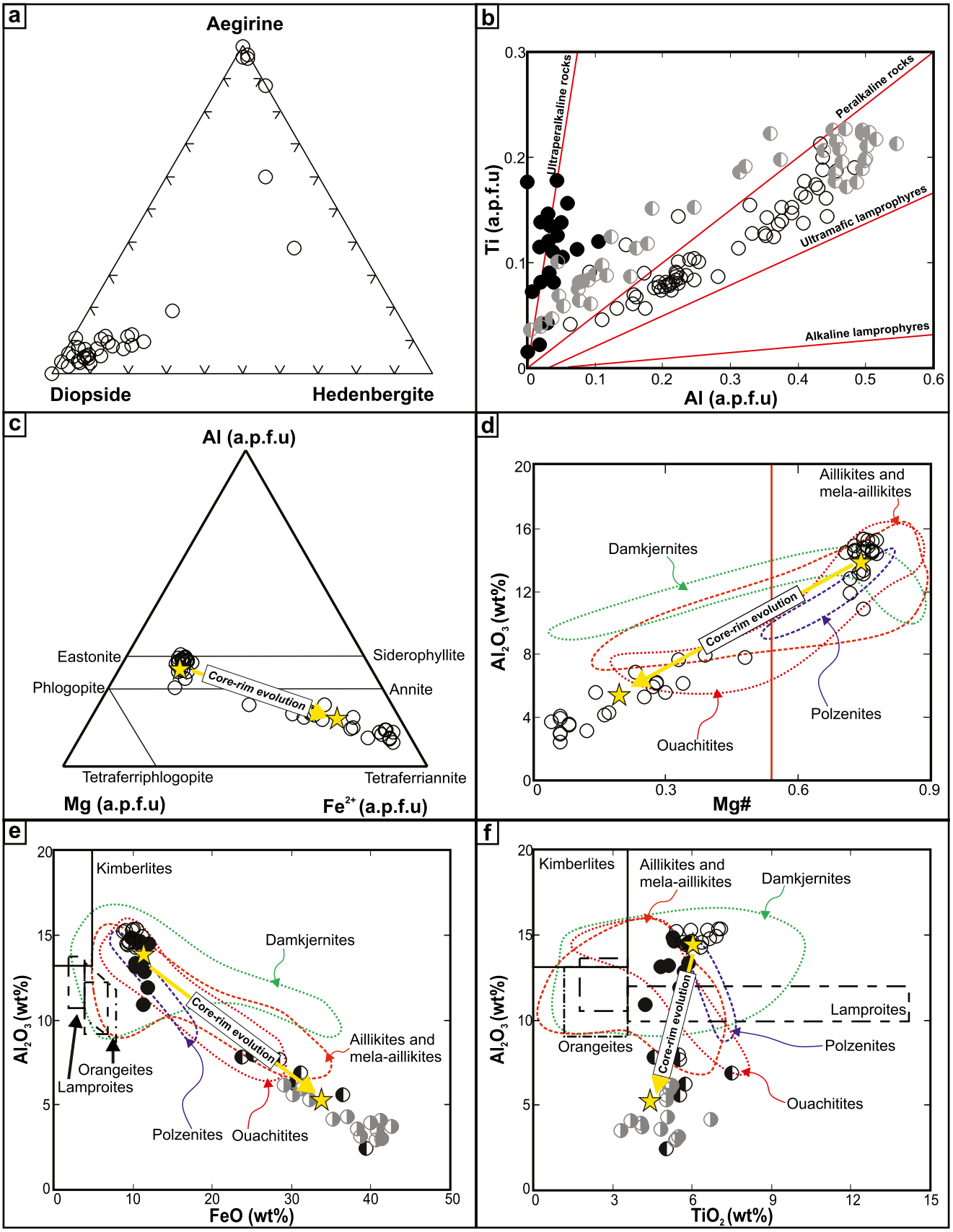
a
Aegirine
Diopside
Hedenbergite
b
Ti (a.p.f.u)
Al (a.p.f.u)
Ultraperalkaline rocks
Peralkaline rocks
Ultramafic lamprophyres
Alkaline lamprophyres
c
Al (a.p.f.u)
Eastonite
Siderophyllite
Phlogopite
Annite
Core-rim evolution
Tetraferriphlogopite
Tetraferriannite
Mg (a.p.f.u)
Fe2+ (a.p.f.u)
d
Al2O3 (wt%)
Mg#
Aillikites and mela-aillikites
Damkjernites
Core-rim evolution
Polzenites
Ouachitites
e
Al2O3 (wt%)
FeO (wt%)
Kimberlites
Damkjernites
Core-rim evolution
Aillikites and mela-aillikites
Orangeites
Lamproites
Polzenites
Ouachitites
f
Al2O3 (wt%)
TiO2 (wt%)
Kimberlites
Aillikites and mela-aillikites
Damkjernites
Lamproites
Orangeites
Core-rim evolution
Polzenites
Ouachitites

◂**Fig. 5** **a** Aegirine-diopside-hedenbergite diagram for clinopyroxenes of Mt. La Queglia (Reguir et al. 2012). **b** Plot of Ti versus Al for clinopyroxenes of Mt. La Queglia. The black circles represent the aegirine compositions; the grey circles are the clinopyroxene from rock-type 2, and the empty circles are the clinopyroxene from rock-type 1. Lines for alkaline and ultramafic lamprophyres are from Mitchell (2009) and lines for peralkaline and ultraperalkaline rocks are from Stoppa and Cundari (1998). **c** Mg–Fe^{2+}–Al classification diagram for micas. **d** Al_2O_3 versus Mg# discrimination plot (Rock 1986). Compositional fields for aillikites, mela-aillikites, polzenites, ouachitites, and damkjernites are from Malpas et al. (1986); Delor and Rock (1991); Hoch (1999); Tappe et al. (2004, 2006); Ulrych et al. (2008); Zappettini et al. (2015) and Kargin et al. (2017). **e** Al_2O_3 versus FeO, and **f** Al_2O_3 versus TiO_2 variation plots for mica (Mitchell 1995). Compositional fields for aillikites, mela-aillikites, polzenites, ouachitites, and damkjernites are the same as in panel **d**

and menisci-linked, and about 0.5 cm in size. The ocelli can make up to 25 vol% of the rock in places. They are composed of Sr-rich calcite with rims outlined by tangentially arranged tiny crystals of aegirine and mica. Part of the structure can be contoured by acicular aegirine, growing perpendicular from the rim towards the centre of the ocellus. Ocelli cores are composed of mosaic textured carbonate minerals and long needles of apatite, with subordinate K-feldspar and zeolites. Calcite contains a myriad of exsolved strontianite which concentrate at crystal boundaries. The ocelli concentration towards the contact indicates primary carbonate migration towards the cold contact. Calcite is also present as intergranular material and the total amount of calcite in the rock is 47 vol% by XRPD. The dominant mafic minerals are diopside (28 vol%), phlogopite (8 vol%), chlorite as alteration product of the groundmass (13 vol%) and minor amounts of perovskite (2 vol%).

Rock-type 2, facies c (section QN1, QN2) (Fig. 4a and b): This is a spinifex textured rock which shows the typical quench texture formed by sheaf-spherulitic diopside-grossmanite (10 vol% by XRPD) and with feathery, curved-branching phlogopite immersed in a groundmass of nepheline (17 vol%) and calcite. Calcite is to 32 vol%, indicating that this rock has a carbonatitic affinity. Andradite (10 vol%), perovskite (2.3 vol%), Ti–rich magnetite, hydroxylapatite (2.7 vol%), K-feldspars, chabazite-Ca, and alteration phases (phengite and chlorite) form the rest of the rock.

Rock-type 2, facies d (VT 22-6a, VT 22–3) (Fig. 4c and d): This facies has a microporphyritic intergranular texture and consists of abundant prismatic elongate clinopyroxene, phlogopite-biotite with intergranular carbonate and nepheline plus apatite and spinel. K-feldspar is also present and forms spherulitic aggregates or patches with aegirine, micas and apatite.

Rock-type 3, hydrothermal facies (Q1, Q2, Q20a, IT-22–7, Q12, Q8) (Fig. 4e and f): This facies is holocrystalline and coarse-grained, with an equigranular and autoallotriomorphic texture, and a banded structure. The major mineral is calcite, followed by fine-grained intergranular, cauliflower-shaped, zoned glauconite, and a mixture of spinel group mineral and Ti–rich magnetite plus chabazite. Glauconite and spinel infiltrate the calcite grains and fill fractures, with typical cauliflower concretional shape. Chabazite is euhedral and seems to have co-precipitated with calcite. Glauconite appears anhedral and shows a slight pleochroism from yellow to emerald-green to brownish. Patches near veins from hydrothermal rocks are composed of transparent mosaic textured calcite and chabazite. Representative compositions of mineral phases are provided in Supplementary Table S2.

Clinopyroxene

Clinopyroxene compositions range from diopside to aegirine (Fig. 5a). Phenocryst rims and groundmass clinopyroxenes range from aegirine-augite to aegirine (26–91 mol.% $NaFeSi_2O_6$) and are characterized by high molarTi/Al values (0.9–6.4) typical of a peralkaline crystallisation environment. Si + Al in the T site is generally < 2 a.p.f.u.. Nevertheless, some samples belonging to rock-type 1 (QN14, QN128, QN41, QN167) have Si a.p.f.u. < 1.44 thus allowing Ti entering this site, up to 0.13 a.p.f.u.

The composition of diopside in rock-type 1 shows a lower content of TiO_2 (on average, 4.0 in rock-type 1 and 5.1 in rock-type 2) and molar Ti/Al ratio (on average, 0.9 in rock-type 1 and 1.1 in rock-type 2) and a higher Mg# with respect to rock-type 2 (on average 61 in rock-type 1 and 58 in rock-type 2). Diopside in carbonate segregation patches has higher TiO_2 and FeO and a lower MgO content compared with the other diopside compositions.

Fresh diopside (Fig. S2a and b) with Mg# > 95 may be a good candidate for mantle xenocrysts, but these grains generally have low Cr_2O_3 (max 0.46 wt%) and do not show evidence of disequilibrium, such as embayment or coronas. According to Zhang and Liou (2003), Ti solubility in clinopyroxene increases with temperature and decreases with pressure. Their composition confirms they are high temperature liquidus minerals with high Ti/Al (≅ 0.5), a typical value for ultramafic lamprophyres, whereas mantle xenocrysts should have Ti/Al < 0.2 (Cundari and Ferguson 1982). The TiO_2 content of Mt. La Queglia clinopyroxene is exceptionally high for a terrestrial clinopyroxene and, in addition, is remarkably high in Al_2O_3 (> 10 wt%). This composition exceeds the maximum content reported in the literature (7.4 wt%; Rock 1991). Ti/Al molar ratio greater

than 0.5 is typical of peralkaline and ultra-peralkaline rocks (Stoppa and Cundari 1998).

Clinopyroxene shows oscillatory zoning for Ti and a decrease in Ti/Al from core to rim. Late-stage clinopyroxene shows relatively low Ti compared with diopside cores. Lower Ti rims are related to the crystallisation of perovskite and an unidentified TiO_2 polymorph. In a Ti versus Al diagram (Fig. 5b), clinopyroxenes show three distinct trends. The first, typical of aegirines, is represented by a substantial increase in Ti, typically observed in ultra-peralkaline rocks (Mitchell 2009). The second and third, with a parallel trend, follow an enrichment towards higher values of Ti and Al, characterising peralkaline to ultramafic rocks. This distribution is not observed in alkaline lamprophyres and Roman Region rocks, which have a much lower Ti content (Stoppa et al. 2003; Panina et al. 2003).

Micas

Mica usually forms euhedral crystals only in the groundmass, but long laths are present and sometimes abundant in segregation patches. In this case, they are mantled by aegirine.

Mica cores are near eastonite end-member (Fig. 5c). Al_2O_3 is between 10.8–15.4 wt%, TiO_2 ranges from 4.22 wt% and 7.08 wt% and FeO between 8.84 and 12.0 wt%. BaO is up to 3.90 wt% and F up to 1.10 wt%. Mg# is between 71-78. Rims are near to tetraferriannite end-member (Fig. 5c). These micas have Al_2O_3 between 2.43

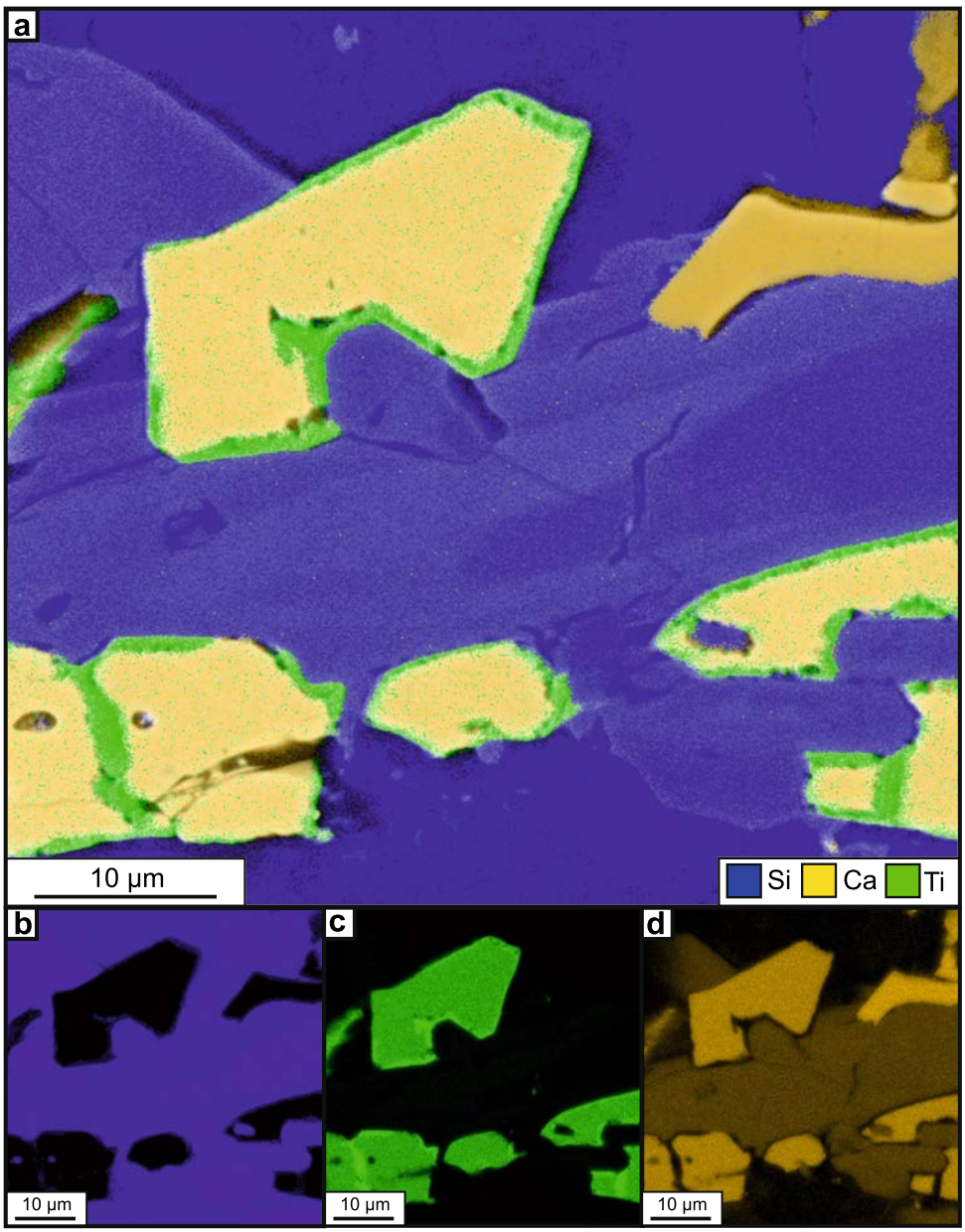

Fig. 6 BSE-EDS map of diopside, an unidentified TiO_2 polymorph and perovskite. The clinopyroxenes (in blue) shows oscillatory zoning and rims depleted in Ti. Perovskite (in yellow) shows an unidentified TiO_2 polymorph rim (in green)

wt% and 7.97 wt% and inversely correlates with FeO (up to 42.5 wt%) and MnO (up to 1.36 wt%). TiO_2 is between 3.30 wt% and 7.50 wt%, F is up to 0.64 wt% and BaO reaches up to 1.50 wt%. Mg# ranges from 48 to 5. Al_2O_3 content positively correlates with Mg#, moving from the rims to the cores (Fig. 5d). The T-site is always saturated in both the cores and the rims.

Crystallization trends show an increase in Si (from 4.9–5.5 a.p.f.u. in cores to 5.5–5.9 a.p.f.u. in rims), Fe_t (from 1.1–1.5 a.p.f.u. in cores to 2.9–6.0a.p.f.u in rims) and Mn (from 0.01–0.03 a.p.f.u. in cores to 0.06–0.19 a.p.f.u. in rims) and a related decrease in Mg (from average of 3.8 a.p.f.u. in cores to 0.3–2.7 a.p.f.u. in rims) and Ba (from 0.1–0.2 a.p.f.u. in cores to 0.03–0.09 a.p.f.u. in rims). Similar Al_2O_3-rich phlogopites are widespread in lamprophyres (Rock 1991).

The evolution trend in respect to Al_2O_3 versus Mg# and Al_2O_3 versus FeO is similar to that observed in ouachitites (Fig. 5e and f), whereas the decrease of Al_2O_3 and TiO_2 seems unique to the Mt. La Queglia micas.

Garnet

Garnets from Mt. La Queglia rocks are molar solutions between $\{Mg_3\}[Al_2](Si_3)O_{12}$ pyrope (20–37 mol%), $\{Ca_3\}[Fe_2](Si_3)O_{12}$ andradite (12–33 mol%), $\{Ca_3\}[TiFe](Si_3)O_{12}$ morimotoite (8–30 mol%), and $\{Ca_3\}[Al_2](Si_3)O_{12}$ grossular (8–16 mol%) plus minor $\{Ca3\}[Ti_2](SiFe_2)O_{12}$ schorlomite, $\{Mn_3\}[Al_2](Si_3)O_{12}$ spessartine and $\{Fe_3\}[Al_2](Si_3)O_{12}$ almandine molar solution. TiO_2 contents range from 5.8 wt% to 8.3 wt%. Fe^{3+}/Ti in the octahedral position can be > 1, as in samples Q6-52, Q6-47, Q6-53, Q6-55, QN-G49, QN-G50, QN-G51 and QN-G52 (schorlomite), or < 1, as in samples Q6-51 andQ6-61 (melanite). Mg# is between 77 and 93.

Perovskite

Euhedral perovskite crystals grow at the contact with clinopyroxene. Notably, they show an unidentified TiO_2 polymorph rim (Fig. 6). Their composition is 0.2–0.5% lueshite, 0.9–3.3% loparite, 0.2–0.5% tausonite, and 96.7–97.7% perovskite sensu stricto. Low Fe and Na contents are common in perovskite from ultramafic rocks across the board (clinopyroxenites, katungites, kimberlites, etc.). Nb_2O_3 is found in perovskite up to 0.5 wt% and Ta_2O_5 is near detection limit.

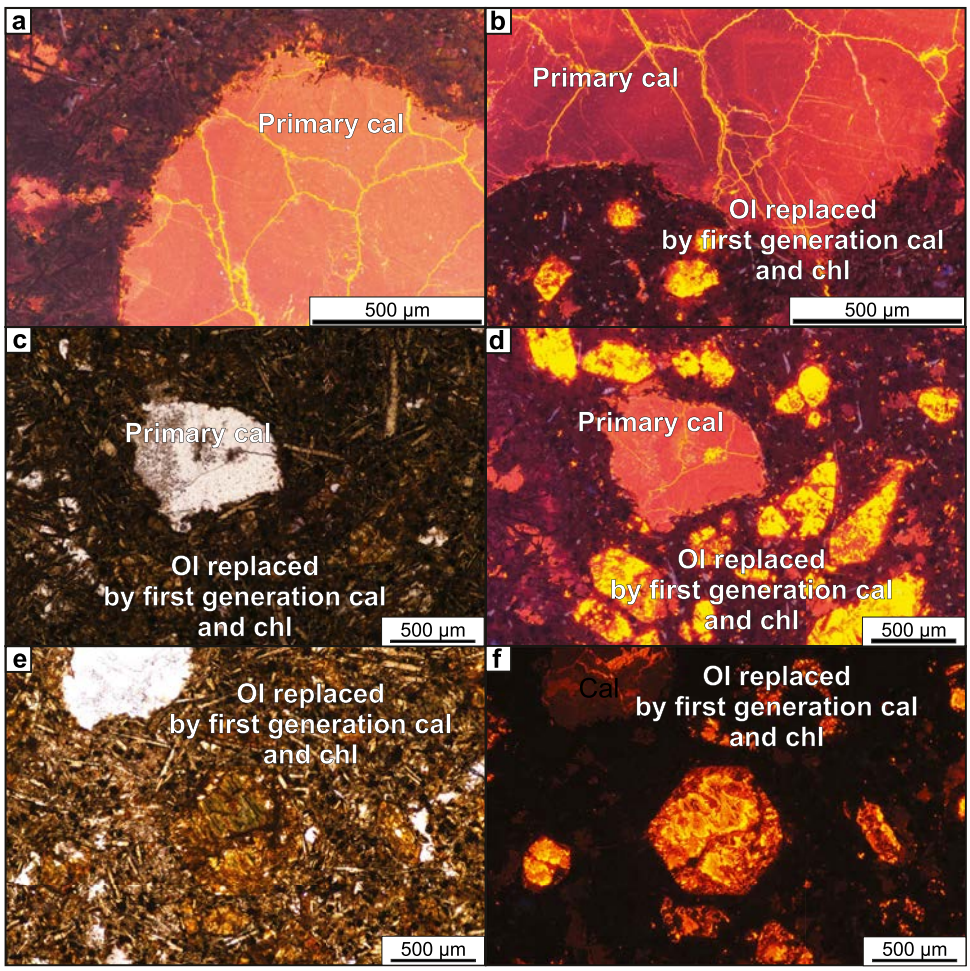

Fig. 7 Plane polarised light (PPL) and cathodoluminescence (CL) images of Mt. La Queglia rocks. **a-b** Detail of a carbonate ocellus in the matrix, showing the three generations of carbonate in Mt. La Queglia Q6 rock. **c** PPL image and **d** CL image of Mt. La Queglia rock Q6. **e** PPL image and **f** CL image of olivine replaced by calcite and chlorite from Mt. La Queglia rock Q6

Table 1 Whole-rock analyses results of Mt. La Queglia rock-types 1, 2 and 3

Sample	Rock-type 1				Rock-type 2						Hydrothermal carbonatite
	Q3	DUP-Q3	Q5	Q6	It22/1	It22/2	It22/3	It22/4	It22/5	It22/5a	It 22/7
Major oxides (wt%)											
SiO_2	36.1	36.6	36.9	33.5	37.3	35.3	35.8	34.9	35.7	34.9	1.85
TiO_2	3.48	3.55	3.75	3.52	4.15	3.64	3.74	3.6	3.79	3.78	0.07
Al_2O_3	9.81	9.80	8.31	7.74	12.0	12.6	12.6	12.5	11.9	11.0	0.40
Fe_2O_3	6.37	6.60	8.08	5.91	8.03	7.40	7.83	7.23	7.77	7.72	0.83
FeO	3.70	3.70	3.40	4.10	3.41	3.05	3.41	3.23	3.05	3.23	0.15
MgO	12.5	12.6	10.8	13.1	12.0	13.2	13.6	13.9	10.7	17.9	1.00
CaO	13.4	13.5	14.3	15.3	8.77	6.89	6.93	6.98	12.3	8.50	53.3
Na_2O	0.89	0.88	0.44	0.68	4.15	0.59	1.58	0.74	1.99	1.47	0.01
K_2O	1.25	1.23	0.90	0.91	0.66	2.88	2.08	2.73	1.64	0.69	0.24
P_2O_5	1.40	1.42	1.14	1.04	1.52	1.57	1.5	1.61	1.49	1.32	0.10
CO_2	3.09	3.07	3.21	5.60	0.48	1.60	1.57	1.52	1.69	0.42	42.0
Total	91.9	93.0	91.2	91.5	92.6	88.7	90.7	89.0	92.0	90.9	100
Mg#	85.8	85.8	85.0	85.1	86.3	88.5	87.7	88.4	86.3	90.8	92.2
Ca#	43.4	43.6	48.7	45.7	34.4	27.3	26.8	26.6	45.1	25.4	97.5
Trace elements (ppm)											
Be	3.00	3.00	2.00	2.00	2.42	3.06	2.77	2.48	2.65	2.75	n.a
V	316	318	264	251	416	507	590	450	416	404	n.a
Cr	295	296	720	671	156	9.40	10.6	8.50	54.0	182	n.a
Co	38.9	40.7	50.0	49.4	37.0	27.0	30.0	26.0	34.0	38.0	n.a
Ni	170	174	379	341	170	69.0	72.0	63.0	116	160	n.a
Cu	64.7	67.9	38.7	47.2	60.0	112	107	108	57.0	52.0	n.a
Zn	91.8	91.3	100	81.8	99.0	92.0	78.0	73.0	103	102	n.a
Ga	19.0	20.0	16.0	14.0	17.0	21.0	21.0	19.0	20.0	18.0	n.a
Ge	n.a	n.a	n.a	n.a	1.13	1.10	0.99	1.04	1.04	1.14	n.a
Rb	43.0	43.0	26.0	32.0	32.0	72.0	45.0	69.0	49.0	29.0	n.a
Sr	817	812	611	616	894	1484	510	928	1098	700	160
Y	28.8	29	26.2	22.8	30.0	28.0	29.0	26.0	32.0	28.0	9.08
Zr	372	368	338	307	455	176	521	560	149	141	9.46
Nb	143	148	136	119	125	5.10	21.0	113	88.0	4.91	n.a
Mo	n.a	n.a	n.a	n.a	0.16	0.22	0.26	0.20	0.38	0.45	n.a
Sn	2.00	3.00	2.00	2.00	2.17	0.36	1.06	2.46	1.4	0.28	n.a
Cs	0.60	0.70	0.50	0.40	0.34	0.41	0.70	0.30	0.30	0.30	n.a
Ba	848	851	498	617	1455	1618	1852	1500	1103	712	28.2
La	90.0	94.3	107	94.5	64.0	42.0	46.0	41.0	60.0	52.0	49.6
Ce	160	169	215	188	113	63.0	69.0	61.0	100	93.0	84.5
Pr	15.4	15.6	21.2	18.8	12.7	6.50	7.20	6.20	10.8	10.6	8.79
Nd	65.3	64.5	89.1	78.8	49.0	24.0	27.0	24.0	41.0	40.0	35.8
Sm	12.5	12.4	16.2	14.3	9.60	5.60	5.80	5.20	8.50	8.30	5.14
Eu	3.67	3.69	4.40	3.97	3.08	2.01	2.18	1.90	2.73	2.62	1.41
Gd	10.8	10.8	12.8	11.7	9.30	6.30	6.60	5.80	8.50	8.00	4.51
Tb	1.44	1.46	1.61	1.48	1.19	0.88	0.87	0.80	1.12	1.02	0.46
Dy	7.36	7.38	7.44	6.79	6.00	5.00	5.00	4.61	5.80	5.50	2.27
Ho	1.20	1.18	1.14	1.03	1.03	0.89	0.92	0.81	1.03	0.94	0.36
Er	3.10	3.13	2.92	2.66	2.62	2.34	2.41	2.15	2.60	2.30	0.87
Tm	0.41	0.402	0.36	0.35	0.31	0.30	0.31	0.28	0.32	0.29	0.08
Yb	2.30	2.29	2.05	1.8	1.87	1.78	1.82	1.68	1.90	1.70	0.44

Table 1 (continued)

Sample	Rock-type 1				Rock-type 2						Hydrothermal carbonatite
	Q3	DUP-Q3	Q5	Q6	It22/1	It22/2	It22/3	It22/4	It22/5	It22/5a	It 22/7
Lu	0.28	0.28	0.25	0.22	0.24	0.26	0.25	0.24	0.26	0.24	0.06
Hf	8.90	8.90	9.10	8.10	7.50	1.42	6.20	9.40	1.87	1.13	n.a
Ta	5.60	5.60	7.00	6.40	4.81	0.12	0.48	2.62	2.88	0.20	n.a
Pb	3.00	3.00	bdl	bdl	5.50	4.41	9.00	4.55	4.62	3.95	n.a
Th	8.26	8.31	13.6	11.9	7.10	1.54	1.79	1.51	4.50	6.20	0.06
U	3.10	3.24	1.95	2.27	2.91	3.16	3.23	3.45	2.63	2.68	0.23

n.a. not analyzed, *Mg#* Mg number 100*Mg/(Mg + Fe^{2+}), *Ca#* Ca number 100*Ca/(Ca + Mg)

Spinel group

Spinel cores are a solid solution of 31 mol % spinel sensu stricto and 32% magnesio chromite, with 9 mol% hercynite, Mg-ferrite, and chromite, respectively. $Fe^{2+}/(Fe^{2+} + Mg)$ is 0.2. Spinel cores have very low Ti/Ti + Al + Cr (average 0.03) and Cr/Cr + Al of about 0.5, typical of spinels from ultramafic lamprophyres. Spinel rims are magnetite 48 mol.%, magnesioferrite 18 mol.% and ulvöspinel 16 mol.% solid solutions, with minor hercynite and qandilite. $Fe^{2+}/(Fe^{2+} + Mg)$ is between 0.2–0.9 and Cr/(Cr + Al) is always < 0.1.

Apatite

Apatite forms inclusions in melilite and mica crystals and is present as abundant long (up to 6 mm) acicular crystals in the groundmass. It classifies F-rich hydroxylapatite. $La_2O_3 + Ce_2O_3$ is up to 0.2 wt%; F is between 1.3 and 1.90 wt%, and Cl is up to 0.3 w%. SiO_2 ranges between 1.6 and 3.5 wt%, and SO_3 is up to 1.5 wt%. SrO is usually between 0.4 and 1.2 wt%. The Si-P-S site is always undersaturated, suggesting the presence of CO_2 (Stoppa and Liu 1995). High-Sr apatite up to 2 wt% is typical of apatite in lamprophyres (Rock 1991; Edgar 1989), in carbonatites (Kapustin 1977), and some kamafugitic rocks (Stoppa et al. 2002). F, Cl, and OH are intermediate between kamafugites and carbonatites (Stoppa and Liu 1995).

Calcite

In the analysed samples, calcite is present in different generations and the following order of crystallisation: (i) calcite pseudomorphs of olivine and melilite; (ii) microphenocrysts and intergranular calcite in the groundmass and the ocelli rims; (iii) segregation patches in the groundmass and ocelli cores.

Details on the texture, geochemistry, and origin of carbonate in Mt. La Queglia dyke and Italian lamprophyres are given in Vichi et al. (2005). Further information is given by cathodoluminescence images (Fig. 7), which also reveal minimal compositional differences in calcite.

The euhedral (olivine) grains are the most striking initial feature. These have been replaced, in part, by calcite. The replacement calcite probably represents the earliest generation. Calcite in the groundmass is much darker red in CL images. This appears similar in luminescence to the outer-most carbonate generation (i.e., closest to the edge) in the ocelli. Most ocelli are composed of zoned bright red/orange calcite. Zoning indicates growth from the outside into the middle. Lastly, there are bright orange fractures and, locally, bright orange luminescent cores. The low variation in cathodoluminescence intensity and colour in the calcite grains probably reflects minimal variation in MnO, FeO and La_2O_3 contents, as supported by microprobe analysis. Calcite in the groundmass underwent recrystallisation at a late stage, producing strontianite exsolution (Vichi et al. 2005).

K-Feldspar

Euhedral K-feldspar is found only in segregation patches and rarely in the groundmass, co-precipitating with carbonate. Their composition is in the range $Or_{92–98}$ and is characterised by Fe_2O_3 from 0.2–0.9 wt% and BaO up to 1.2 wt%. CaO is always < 0.1 wt% and Na_2O is between 0.2–0.9 wt%, corresponding to Ab ranging from 1.9 to 8. K-feldspar in ultramafic lamprophyres is only typically noted in damkjernites, where k-feldspar is associated with nepheline (Rock 1991), as is also the case for the Mt. La Queglia rocks.

Nepheline

Nepheline is present as rare euhedral crystals in the groundmass (Fig. S2c and d). The Na_2O content is between 11–14 wt%, K_2O about 8.8 wt% and Fe_2O_3 about 2.6 wt%. Among ultramafic lamprophyres, nepheline is known only from damkjernite, ouachitite, and alnÖite. High Q% (average 6.49) in nepheline from La Queglia rocks indicates that they formed in early high-T crystallization conditions They fall into the field of nepheline + feldspar stability (Deer et al. 1997) as demonstrated by the co-precipitation relationship with feldspar.

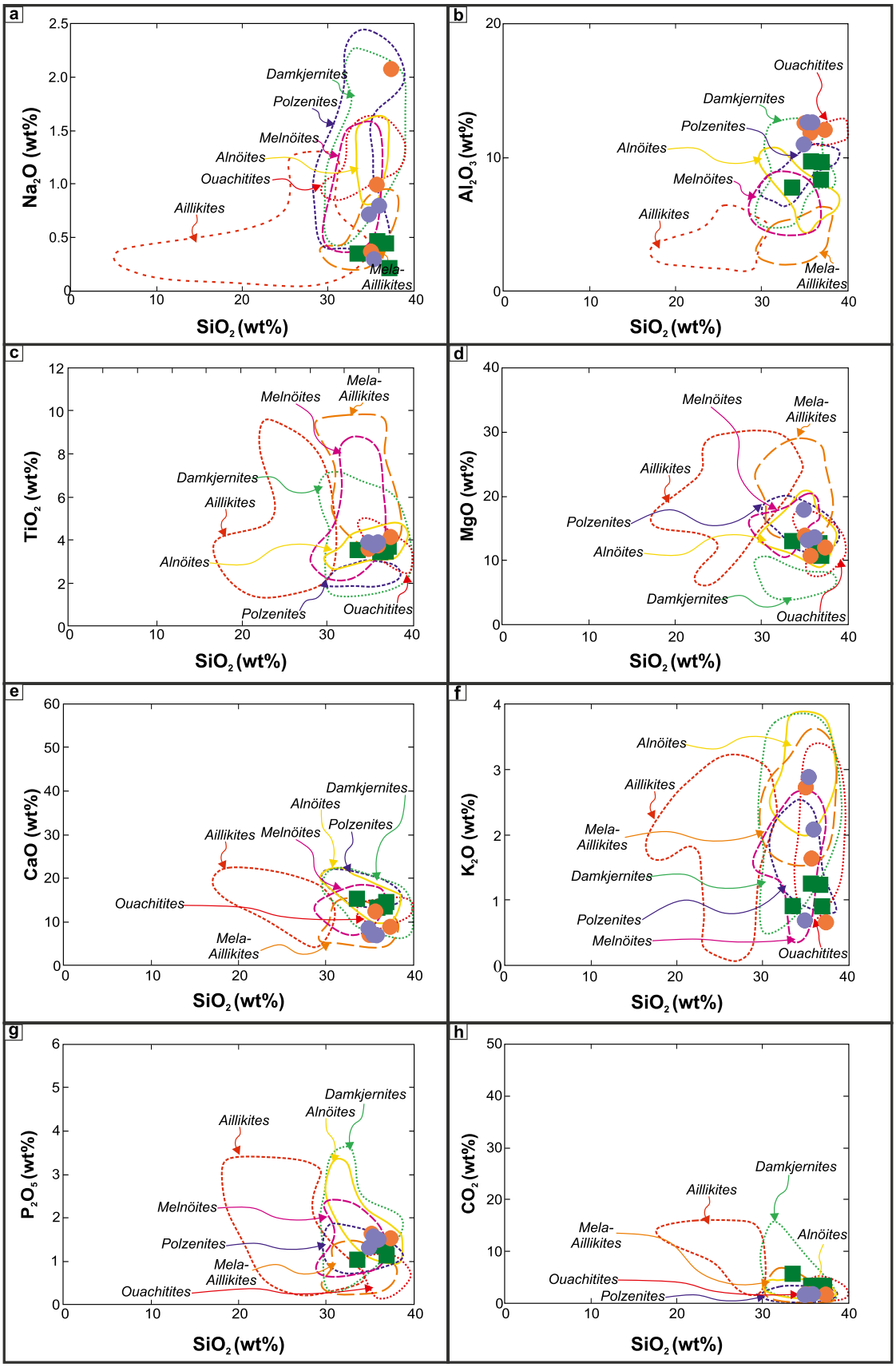
a
Na2O (wt%)
SiO2 (wt%)
Damkjernites
Polzenites
Melnöites
Alnöites
Ouachitites
Aillikites
Mela-
Aillikites
b
Al2O3 (wt%)
SiO2 (wt%)
Ouachitites
Damkjernites
Polzenites
Alnöites
Melnöites
Aillikites
Mela-
Aillikites
c
TiO2 (wt%)
SiO2 (wt%)
Mela-
Aillikites
Melnöites
Damkjernites
Aillikites
Alnöites
Polzenites
Ouachitites
d
MgO (wt%)
SiO2 (wt%)
Melnöites
Mela-
Aillikites
Aillikites
Polzenites
Alnöites
Damkjernites
Ouachitites
e
CaO (wt%)
SiO2 (wt%)
Damkjernites
Alnöites
Aillikites
Melnöites
Polzenites
Ouachitites
Mela-
Aillikites
f
K2O (wt%)
SiO2 (wt%)
Alnöites
Aillikites
Mela-
Aillikites
Damkjernites
Polzenites
Melnöites
Ouachitites
g
P2O5 (wt%)
SiO2 (wt%)
Damkjernites
Alnöites
Aillikites
Melnöites
Polzenites
Mela-
Aillikites
Ouachitites
h
CO2 (wt%)
SiO2 (wt%)
Damkjernites
Aillikites
Mela-
Aillikites
Alnöites
Ouachitites
Polzenites

◂**Fig. 8** Plot of major oxides versus SiO_2 (Zozulya et al. 2020) for Mt. La Queglia lamprophyres. Compositional fields for aillikites, mela-aillikites, melnoites, alnöites, damkjernites, polzenites, and oauchitites are from Malpas et al. (1986); Delor and Rock (1991); Barbieri et al. (1997); Le Roex and Lanyon (1998); Hoch (1999); Graham et al. (2002); Rileya et al. (2003); Tappe et al. (2006); Ulrych et al. (2008; 2014) and Kargin et al. (2017). Symbols: green squares are rock-type 1; orange circles are rock-type 2, facies c; violet circles are rock-type 2, facies d

Zeolites

Zeolites are present in the groundmass, segregation patches, and at the edge of ocelli structures. The zeolite-group minerals are close in composition to chabazite, which occurs in association with hydrothermal-metasomatic minerals, such as carbonate.

Glauconite

The SiO_2 content of glauconite varies from 45 to 59 wt%, Al_2O_3 from 4.4 to 10.5 wt% and FeO from 10.6 to 37.8 wt%. Al_2O_3 and FeO negatively correlate, and the Al and Si content is enough to saturate the tetrahedral site. This mineral shows a concretionary structure and appears zoned, with increasing Si and Mg content from the core toward the edge. Al shows a more homogenous distribution though it also shows a more marked abundance in the edge of the mineral. Conversely, Fe shows a higher concentration from the edge to the core. Ti–rich magnetite grains are also more concentrated in the mineral core due to the higher concentration of Fe. Magnetite spinel in the hydrothermal facies is poor in Ti and rich in Mg, Al, and Si. So, it is a molar mixture of magnetite and other spinel group minerals. The presence of glauconite, which is more commonly linked to sediment diagenesis, is also described in basalts and other mafic rocks which have undergone hydrothermal alteration (Alt et al. 1992).

Bulk rock geochemistry

Major element geochemistry

The whole-rock major and trace element compositions of the two main rock-types and the hydrothermal 'carbonatite' from La Queglia are presented in Table 1. Rock-type 1ranges from 33.5 to 36,9 wt.% SiO_2 and is potassic [$K_2O > (Na_2O\text{-}2)$, $K_2O/Na_2O = 1.22$]. Al_2O_3 ranges from 7.7 to 9.8 wt%; Fe_2O_3 is between 8.1 wt% and 5.9 wt%, MgO is between 10.8 and 13.1 wt% and CaO is between 13.4 and 15.3 wt%. TiO_2, FeO, $Na_2O + K_2O$, and P_2O_5 are quite constant and average 3.6 wt%, 3.7 wt%, 1.8 wt%, and 1.3 wt%, respectively. CO_2 ranges from 3.1 wt% to 5.6 wt%. The Agpaitic Index (A.I. = molar Na + K/Al) ranges from 0.22 to 0.28. Their Mg# is between 85 and 86. Rock-type 2 has SiO_2 ranging from 34.9 to 37.3 wt% and is potassic [$K_2O > (Na_2O\text{-}2)$, $K_2O/Na_2O = 1.1$]. Al_2O_3 ranges from 11.0 to 12.6 wt%; Fe_2O_3 is between 7.2 wt% and 8.0 wt%, MgO is between 10.7 and 17.9 wt% and CaO ranges from 6.9 to 12.3 wt%. TiO_2, FeO, $Na_2O + K_2O$, and P_2O_5 are constant and average 3.8 wt%, 3.2 wt%, 3.5 wt%, and 1.5 wt%, respectively. CO_2 ranges between 0.4 wt% to 1.7 wt%. The Agpaitic Index ranges from 0.15 to 0.79. Mg# is between 86 and 91. Rock-type 3 has extremely low SiO_2 (1.9 wt%), and contains a very moderate amount of K_2O, Al_2O_3 and Fe_2O_3. Sr contents reach up to 160 ppm; LREE are relatively high (up to 184 ppm) and La/Lu is 827.

The TAS, R1-R2, and RI-RM-RS diagrams are not suitable for volatile-rich rocks. In specific ternary diagrams for lamprophyres, such as Al_2O_3-MgO-CaO and SiO_2/10-CaO-$TiO_2 \times 4$ (Rock 1991), Mt. La Queglia rock-type 1 plot in the alkaline lamprophyre field whereas rock-type 2 plots in the overlying field of UML and alkaline lamprophyres (AL). This is partially inconsistent with the mineralogical assemblage and mineral chemistry which point towards UML. Such a discrepancy suggests the necessity of further investigation into chemical discriminants that may correctly classify the rock as specific UML.

Different UML can be discriminated using Harker diagrams (Fig. 8) (Zozulya et al. 2020). Mt. La Queglia rocks generally show two distinct compositions in Al_2O_3-SiO_2, CaO-SiO_2, Na_2O-SiO_2 and K_2O-SiO_2 diagrams. Mt. La Queglia rocks cluster in the TiO_2 versus SiO_2, MgO versus SiO_2, P_2O_5 versus SiO_2 and CO_2 versus SiO_2 diagrams in the field of oauchitites, alnöites, melnöites and polzenites. In no case are the rocks classified as aillikites. When the two rocks compositions are distinctly separated (Al_2O_3, Na_2O, K_2O), rock-type 1 falls in the melnöites and polzenites field, and rock-type 2 falls mainly in the damkjernite and the ouachitite fields. We note that rock-type 1 plots in the melnöite field and rock-type 2 more frequently plots in the oauchitite field despite a considerable overlap of UML compositions. This is because melnöite is an UML associated with carbonatitic melts and transitions to other UML such alnöite and poltzenite. To clarify the affinity for one of the above UML, we provide a statistical approach based on rank analyses following the Rank analyses for alkaline and carbonatitic rocks (Ambrosio 2020).

Rank analysis

Ambrosio (2020) introduced three different lamprophyre categories: high-Mg, high-Ca, and high-Al. High-Mg lamprophyres are more akin to primary mantle melts and kimberlites; high-Ca lamprophyres are akin to carbonatites, and high-Al lamprophyres are akin to evolved products with involvement of a continental crust component.

Mt. La Queglia rock-types 1 and 2 and melnoites plot 100% in the high-Mg field, whereas about 16% of the other worldwide ultramafic lamprophyres extend to the high-Ca fields (Fig. S1). Olivine melilitites and their potassic variant kamafugites plot in the high-Mg field with a lesser extension in the high-Ca field (~ 11% and 30%, respectively). Italian alkaline lamprophyres plot in both high-Mg (56%), high-Ca (30%), and high-Al fields (13%). The general statistic distribution suggests that the most similar rocks to Mt. La Queglia rock-type 1 are melnoites, while rock-type 2 show the main content of Al_2O_3 and MgO and do not plot in any specific considered rock type field. According to rank analysis, Mt. La Queglia rocks show a unique distribution for the Ti-Na rank concerning the other ultramafic lamprophyres.

Trace element geochemistry

Rock-type 1: Rock 1 has a low Mg# because of the disappearance of fresh olivine, which is also confirmed by the high Ca# (Fig. 9a). The La/Lu ratio negatively correlates with Mg# (Fig. 9b) and positively correlates with Ca# like ΣREEs (Fig. 9c, d and e). Large ion lithophile elements (LILE) are generally one order of magnitude lower in concentration than high field strength elements (HFSE). The rock shows a high HFSE ratio ($HFSE^{5+}/HFSE^{4+}$), and a high Cr + Ni content, positively correlating with Ca# (Fig. 9f). The trace element distribution, normalised to primitive mantle, shows a bell-shaped pattern typical of intraplate rocks (Fig. 10a). The absence of a negative Nb–Ta anomaly and the high TiO_2 content suggests melting of a titanate phase in the mantle source. REE content is up to 481 ppm (Fig. 10b), and La/Lu is up to 430. No apparent Eu anomaly is present.

Rock-type 2: Type 2 has a high Mg# due to the abundance of clinopyroxene with a Mg# > 90 (Fig. 9a). Rock-type 2 shows a varying composition compared with rock-type 1, with a similar correlation between Mg# and Ca# (Fig. 9a). In general, HFSE contents are lower and LILE contents higher, and the $HFSE^{5+}/HFSE^{4+}$ ratio is much lower. The presence of a deep Ta-Nb negative anomaly implies crystal settling of perovskite (Chakhmouradian et al. 2013) and an unidentified TiO_2 polymorph occurred to produce rock-type 2 (Fig. 10a).

The REE distribution defines two main chemical facies with different La/Lu ratios, but the HREE content remains the same (Fig. 10b). However, these are not dilution conditions because the HREE content is similar in all the above rocks. The samples IT22/1, IT22/5, and IT22/5a have a higher La/Lu ratio (in average 237.81) than IT22/2, IT22/3, and IT22/4 (on average 172.12). There is no Eu negative anomaly. The first group has variable Mg# and Ca# values, similar to the second group (Fig. 9a). These are variations due to the patchy texture of the rocks, which have different amounts of olivine and melilite replacement by calcite. From the first facies to the second, there is a drastic decrease in Cr + Ni contents (Fig. 9f). Substantial Cr depletion in rock two is probably linked to chromite crystal settling.

Rock-type 3: Rock-type 3 shows a cross-over with rock-type two at the level of Nd (Fig. 10b). This is a cross-over relationship which may indicate separation of a hydrothermal-carbothermal 'carbonatite' from a rock-type 1 melt. This implies a strong fractionation of LREE in the residual fluids, which precipitated during a carbothermal-hydrothermal stage.

Radiogenic isotope geochemistry

Literature data constrain the Mt. La Queglia rocks to the depleted Sr/Nd quadrant at $^{87}Sr/^{86}Sr$ 0.703429 ± 0.000006 and $^{143}Nd/^{144}Nd$ 0.512891 ± 0.000006 (Avanzinelli et al. 2012) and $^{87}Sr/^{86}Sr$ 0.7031 ± 0.0004 and $^{143}Nd/^{144}Nd$ 0.5030 ± 0.0101 (Bell et al. 2013), suggesting an extreme composition, in terms of depleted mantle end-members, of all the Italian igneous rocks (Bell et al. 2013). We obtained similar values for bulk rock $^{87}Sr/^{86}Sr$ (0.703933), $^{143}Nd/^{144}Nd$ (0.51274) (Fig. 11a). To constrain the dominant mantle end-member and possible metasomatising agent, Sr and Nd isotopes have to be interpreted in light of Pb isotopes which are: $^{206}Pb/^{204}Pb = 20.362 \pm 0.011$, $^{207}Pb/^{204}Pb = 15.696 \pm 0.010$, $^{208}Pb/^{204}Pb = 40.765 \pm 0.032$ (Avanzinelli et al. 2012) and $^{206}Pb/^{204}Pb = 19.94$, $^{207}Pb/^{204}Pb = 15.70$, $^{208}Pb/^{204}Pb = 40.75$ (Bell et al. 2013). Combining Sr and Pb data, La Queglia rocks are near to the composition of HIMU (Fig. 11b and c). Based on the available data for other Eocene Italian lamprophyres on the Adria plate then a trend in these data towards EM1 (Enriched Mantle 1) could be hypothesised.

On the basis of the Sr isotope data, previous authors have suggested contamination could have affected the Mt. La Queglia rocks (Barbieri and Ferrini 1984; Woolley et al. 2005). We analysed the country rock limestone (IT218) to verify a possible contribution of crustal material both by local or mantle phenomena. Eocene limestone contacting the igneous body gives $^{87}Sr/^{86}Sr = 0.707858$, $^{143}Nd/^{144}Nd = 0.51263$, $^{206}Pb/^{204}Pb = 18.975$, $^{207}Pb/^{204}Pb = 15.665$, $^{208}Pb/^{204}Pb = 38.736$. This composition corresponds to EM2 (Enriched Mantle 2) and is far away from any possible trend involving isotope variation among Italian lamprophyres (Fig. 11b and c).

Magma genesis

A highly fractionated REE pattern coupled with low HREE contents implies a low partial melting degree of residual garnet in the source region (Pandey et al. 2017) (Fig. 12a). This composition is similar to other similar lamprophyres from India (e.g., Chalapati Rao et al. 2012) (Fig. 12b). Coeval Italian lamprophyres show a pattern resulting from a convergent increase in mantle enrichment and melting depth (Fig. 12c) (Rosatelli et al. 2007). In the mantle array, Mt.

La Queglia rock-type 1 plots consistent with the diagram in Fig. 12c, between Castelletto di Rotzo lamprophyres and Punta delle Pietre Nere lamprophyres (Fig. 12d). These rocks are typical of intraplate magma source and show a mixed nature between OIB and carbonatites-kimberlites.

Discussion

Ultramafic lamprophyres have a complex and complicated classification primarily based on mineral assemblage and chemistry, and the presence of specific minerals. Moreover,

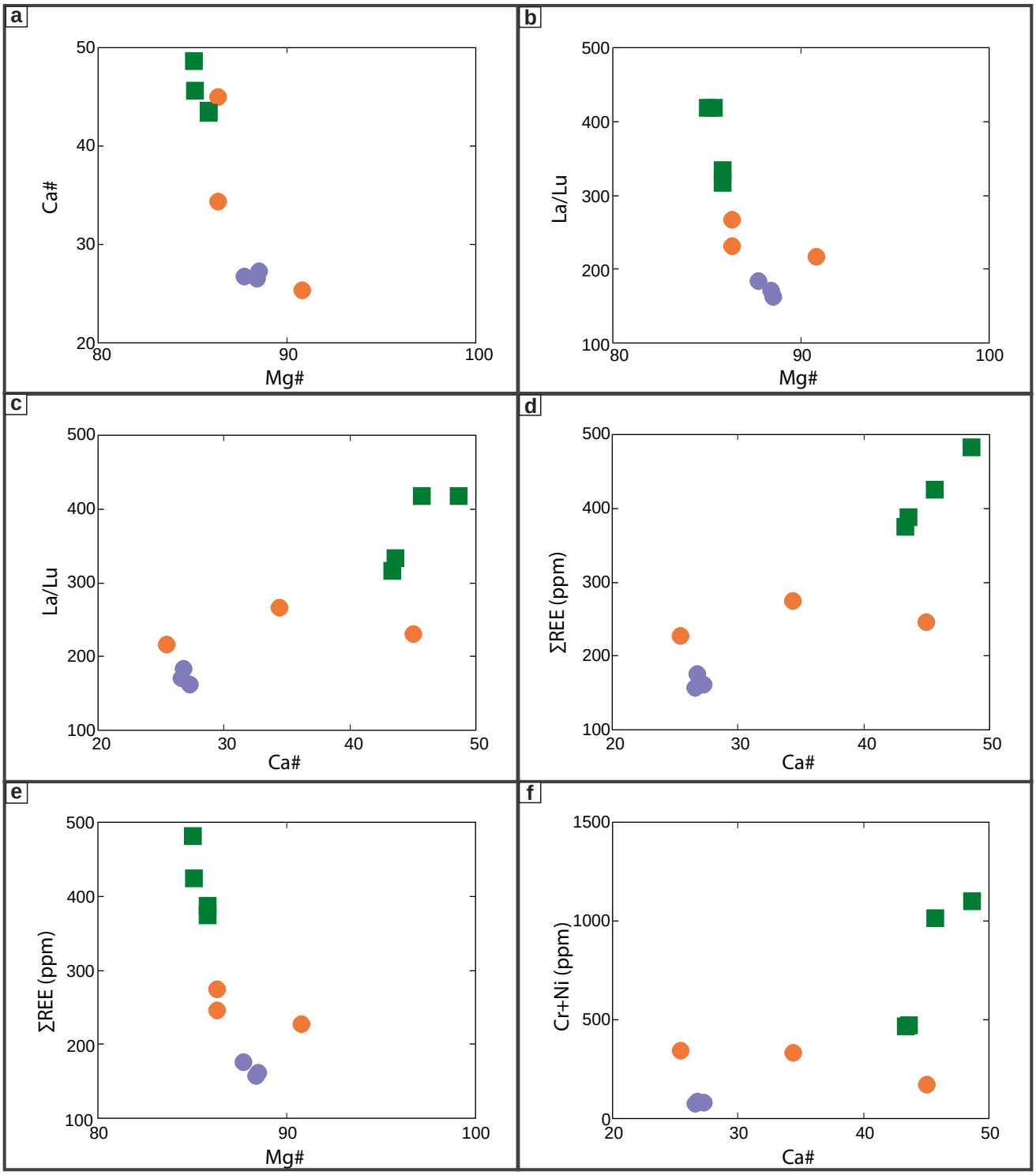

Fig. 9 Trace elements versus Ca# and Mg# variation plots for Mt. La Queglia rock-type 1 and rock-type 2. Symbols as in Fig. 8

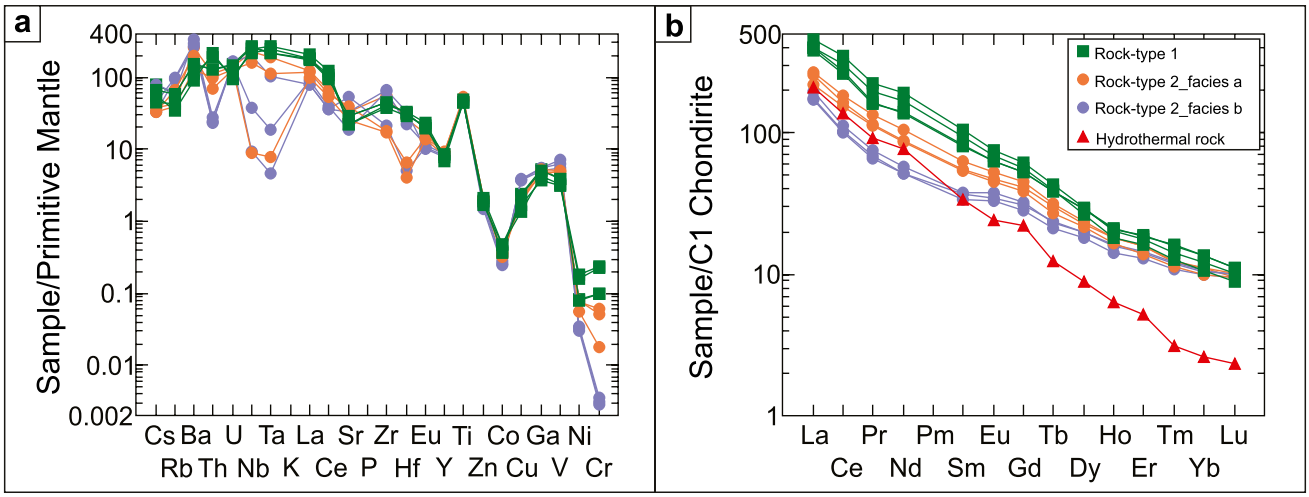

Fig. 10 **a** Primitive-mantle normalised (Wanke et al. 1984; Taylor and McLennan 1985) trace element composition and **b** chondrite normalised (Sun and McDonough 1989) REE patterns of Mt. La Queglia rock-type 1, rock-type 2 facies c and d and rock-type 3

despite a similar composition, a marked polymorphism poses a significant problem in classification. More accurate insight into the Mt. La Queglia rocks reveals textural and compositional variability not described in the previous literature.

There is no evidence of mantle debris in the Mt. La Queglia rocks, despite the finding of mantle nodules in some coeval lamprophyres (Zaccaria et al. 2021). A xenocrystic origin for the olivine is ruled out by several textural features (Fig. S2e and f), such as its perfect euhedral shape, crystallisation in the groundmass, absence of reaction-rims, and the presence of quench features. However, there are no analyses of fresh olivine as it has been completely substituted by primary carbonate. Therefore, the abundance of mafic minerals in equilibrium with the liquidus testifies for a near primary nature of the crystallizing melt of rock-type 1. At Mt. La Queglia, a paucity of hydroxyl-bearing minerals coexists with generalised, pristine olivine and melilite substitution by calcite. CO_2 infiltrating the mantle, within the garnet stability field, can reduce its solidus temperature, producing a breakdown of hydrous minerals, such as amphibole and phlogopite, and stabilizing carbonates (Wyllie and Huang 1975). This explains relatively dry lamprophyres rich in carbonate. Primary carbonate is widespread as an intergranular material, patches, and plastically deformed ocelli. The mineral assemblage suggests a transitional character between an ultramafic lamprophyre (alnöite) and a carbonated olivine melilitite. In Rock's classification of UML (Rock 1991), the term alnöite is referred to rocks carrying biotite, clinopyroxene, melilite, and olivine as essential minerals. Mt. La Queglia rock-type 1 contains only a small amount of mica and very rare amphibole. Therefore, this rock could be considered as a "hydroxyl-poor" UML with only a small amount of hydroxyl-bearing minerals (Rock 1991), and the presence of essential melilite would allow to be classified as melilitite, or carbonated melilitite according to the IUGS classification (Le Maitre 2002; Tappe et al. 2005). Mitchell (1994) and subsequent literature (Graham et al. 2002, 2004; Goto et al. 2004) suggest for the lamprophyric facies with melilite and carbonate the term melnoite, which is also used when the rock cannot be classified with certainty in any of the IUGS UML lithotypes. Therefore, from a merely classificatory purpose, rock-type 1 is now classified as melnöite, a term that refers to a rock that is between an alnoite and an olivine-melilitite, as supported by the statistical analysis of the rock-type 1 chemical analysis (Fig. S1). This overcomes the obstacle of a classification based on melilite abundance, assuming that 10% melilite is a net divide between alnöite and olivine-melilitites (IUGS). On the other hand, the role of carbonate in the petrogenesis of the Mt. La Queglia rocks establishes a further robust link with melnöites.

More primitive samples (rock-type 1) are characterised by low LILE contents, a low $HFSE^{5+}/HFSE^{4+}$ ratio and very high compatible element concentration (Co, V, Ga, Cr, Ni up to 1429 ppm). The texture of these rocks indicates the igneous nature of the carbonate. A high Nb–Ta abundance (average 153 ppm) indicates that early melting has been controlled by a titanate phase in the source region. Low LILE contents can even be due to a source that experienced depletion during an earlier melting event (Mitchell 1995).

Classification of rock-type 2 is not consistent with a melnöite or olivine melilitite and is more similar to a melilite-free UML. However, a specific classification problem remains an open question due to the subtle difference among all these rock types. Notionally rock-type 2 may be classified as ouachitite (melilite-free UML with primary carbonate) because in no case do the rocks plot in the field of the aillikites and have different mineral chemistry. The late-stage minerals formed

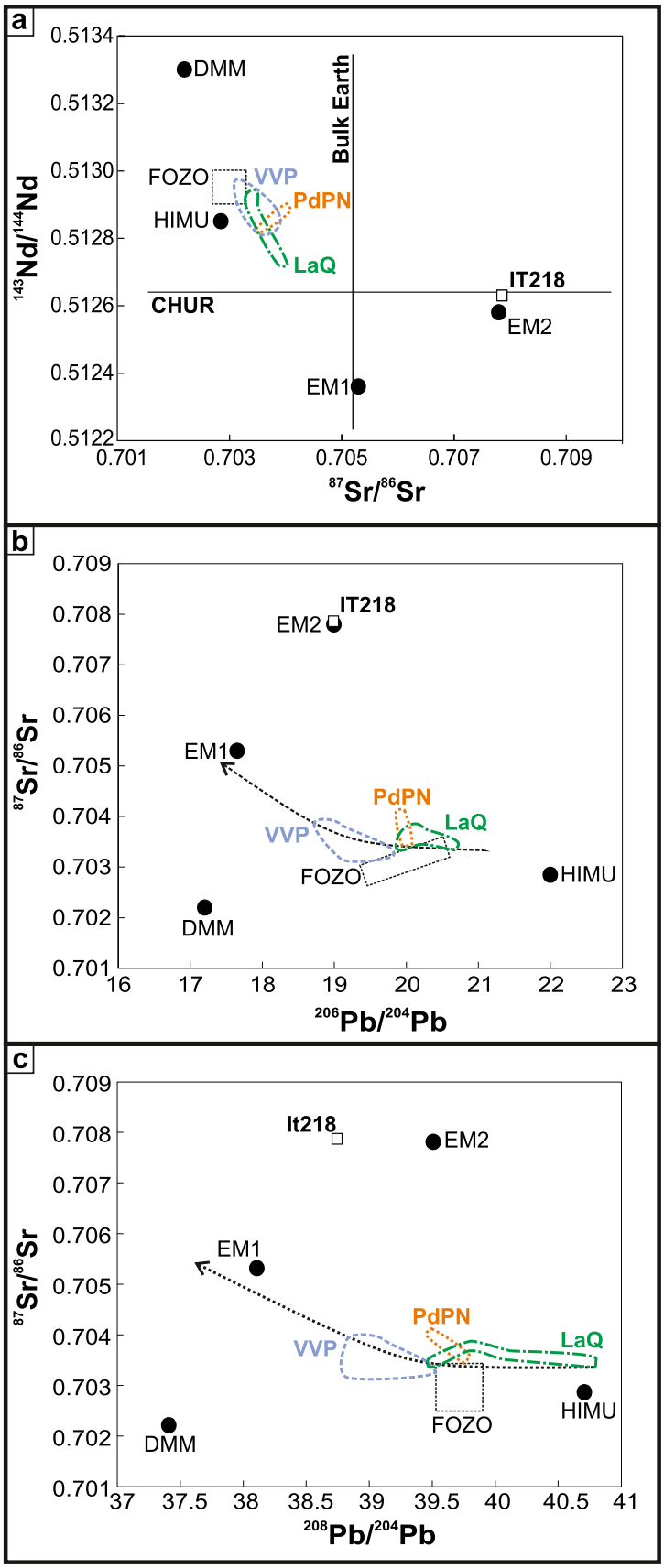

Fig. 11 **a** Conventional $^{143}Nd/^{144}Nd$ versus $^{87}Sr/^{86}Sr$ isotope diagram. The diagram shows DMM, HIMU, FOZO, EM1 and EM2 mantle end-member composition in the depleted mantle isotope quadrant. Compositional field for Mt. La Queglia are from Avanzinelli et al. (2012) and Vichi et al. (2005). The sedimentary limestone country-rocks are new analyses. **b** $^{87}Sr/^{86}Sr$ versus $^{206}Pb/^{204}Pb$ isotope diagram. **c** $^{87}Sr/^{86}Sr$ versus $^{208}Pb/^{204}Pb$ isotope diagram. The spotted line show the trend formed from Etna-Hyblean province and Sardinia Pleistocene rocks (Bell et al. 2013)

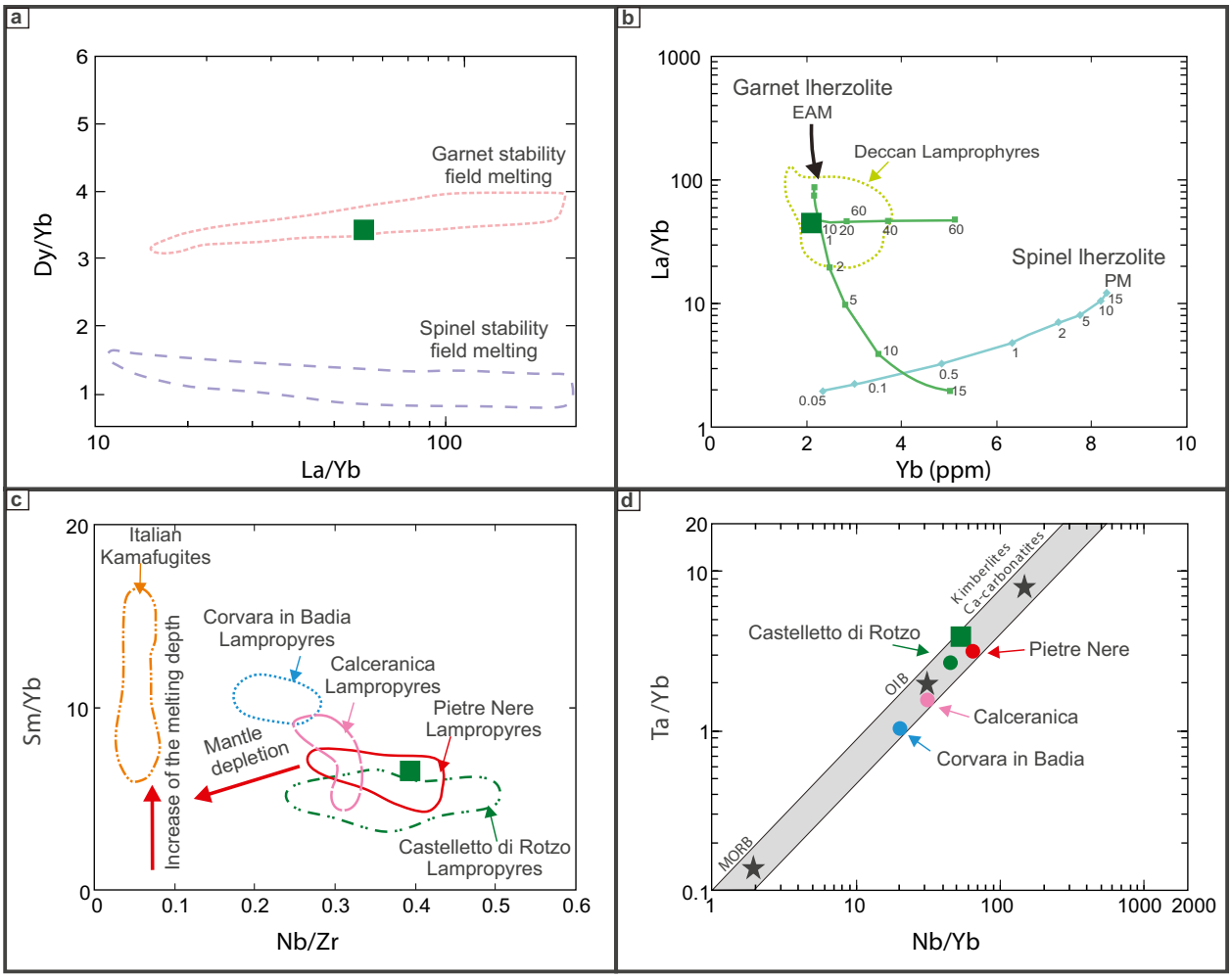

Fig. 12 **a** Dy/Yb versus La/Yb plot (Prelevic et al. 2015). **b** La/Yb versus Y plot (Pandey et al. 2017). **c** Sm/Yb versus Nb/Zr plot (He et al. 2010). Compositional fields are from Stoppa (2008); Stoppa et al. (2016); Stoppa et al. (2019) and Zaccaria et al. (2021). **d** Th/Yb versus Nb/Yb plot (Pearce 2008). The green square represents average compositions of Mt. La Queglia rock-type 1

in the Mt. La Queglia igneous rocks correspond to intergranular phases in the groundmass, segregation patches and ocelli, spinifex clinopyroxene and mica in a calcite groundmass and co-precipitate with felsic minerals observed in rock-type 2. Higher LILEs (Rb, Ba, Sr, Cs), higher $HFSE^{5+}/HFSE^{4+}$ ratio and a very low compatible element' concentration is explained by the appearance of LILE carriers like K-feldspar and the disappearance of perovskite and chromite.

Rock-type 3 seems extremely differentiated, starting from rock-type 1. Despite the mineral assemblage suggesting low-temperature hydrothermal crystallisation conditions, we observe that glauconite and Ti–rich magnetite-ulvöspinel are a late occurrence in the calcite groundmass. This suggests that calcite crystallises early and is probably related to carbothermal residua.

As a whole, the various compositions are not in a dilution-concentration relationship (e.g., not parallel REE distributions) but show some peculiarity linked to silicate-carbonate reaction (Stoppa 2021). In the first crystallisation stage, olivine and melilite are rapidly substituted by calcite. This fact is apparent in the Ca#/Mg# variation, generating the paradox that the most primitive Cr + Ni rich facies have a lower Mg#. The main chemical feature of these rocks is a rapid differentiation that concentrates LREE in the final carbothermal residua. Both mineral compositions and whole-rock compositions suggest evolution from alkaline to metaluminous crystallisation conditions and the loss of alkalis during this process (Rosatelli et al. 2003). LREEs are strongly fractionated, and their lower content in rock-type 2 is compensated by the abundance of LREE in the late-stage carbothermal-residua. This is not surprising as most recent literature indicates that LREEs can be mobile in this condition and transported by fluid (Broom-Fendley et al. 2016; Liu and Hou 2017; Liu et al. 2018).

It is important to assess the role that HIMU has played in Italian magmatism. HIMU component characterises

Mt. La Queglia rocks and it is present in the other igneous rocks of the Adria foreland (Lavecchia and Bell 2012). Thus, the intraplate mantle component HIMU have played a role, likewise EM1, in the magmatic source of in Italy. In fact, the EM1-like component is restricted only to the Plio-Quaternary alkaline lavas from central and northern Sardinia which have the least radiogenic Pb in igneous rocks found in the circum-Mediterranean area (Bell et al. 2013). We suggest a HIMU source, modified by a limited amount of EM1 component. Mt. La Queglia shares a similar isotopic signature with other coeval lamprophyric rocks emplaced on the relatively thick Adria plate, and thus is very different from younger alkaline volcanism in Italy, which postdates the Mediterranean opening and is enriched in Sr. It is possible that HIMU is a very deep signature and EM1 may represent a slightly CO_2 metasomatised ancient lithosphere contribution. The isotope geochemistry and Ta/Yb and Nb/Yb ratios are interpreted as mixture of OIB plus a carbonate-rich component or $CO/HCO_3^-/CO_2$ component to form lamprophyres. Sedimentary limestone has a completely different isotopic composition which rules out any substantial local contamination by sedimentary limestone. In fact, Mt. La Queglia lamprophyres maintain a very primitive HIMU isotopic composition.

Conclusions

An innovative field survey allowed new detailed mapping of Mt. La Queglia outcrops, showing a varied distribution of rock-types. The different rock-types show a marked compositional variability from a near-primary HFSE-rich, Cr-Ni-rich melt to a LREE, and carbonate-rich late-stage differentiate (carbothermal residuum). The petrologic study suggests the combination of two main modifying processes: (1) a reaction between carbonate and silicate liquidus phases and (2) a rapid crystal-settling of perovskite (Chakhmouradian et al. 2013) and Cr-spinel. The main differentiation effects are a decrease in Mg# and increase of Ca# and a significant negative $HFSE^{5+}/HFSE^{4+}$ anomaly plus a dramatic decrease in Cr + Ni. Geochemical data suggest that alkalis and LREE are mobilized by late-stage fluids. However, HREEs remain constant testifying that there is no dilution by external crustal material. In addition, a very large difference in isotopic composition between igneous and sedimentary country rocks completely rules out any local assimilation. From a classification point of view, the most primitive rock-type 1 is a melnoite, whereas rock-type 2 is ouachitite, and rock-type 3 is a hydrothermalised carbothermal-residuum. The general geochemistry of rocks from Mt. La Queglia testifies to an origin from a garnet lherzolite source depleted in LILE with titanates on the liquidus. Isotope compositions clearly indicate a HIMU mantle source for lamprophyric rocks emplaced in the Adria foreland with a possible modest contribution from an EM1 endmember. Ultramafic lamprophyres are challenging rocks, and their evolution opens new frontiers in the interpretation of the relationship between ultramafic silicate rocks and carbonatites and the complex reaction between silicate and carbonate minerals.

Supplementary Information The online version contains supplementary material available at https://doi.org/10.1007/s00710-022-00792-0.

Acknowledgements Constructive reviews by Anton R. Chakhmouradian, Franco Pirajno and an anonymous expert, and helpful comments by guest editor Peter J. Downes, are gratefully acknowledged. Francesco Stoppa thanks the Department of Psychological, Health and Territory Sciences for funding this research.

Funding Open access funding provided by Università degli Studi G. D'Annunzio Chieti Pescara within the CRUI-CARE Agreement.

References

Alt JC, France-Lanord C, Floyd PA, Castillo P, Galy A (1992) Low-temperature hydrothermal alteration of Jurassic Ocean Site 801. In: Larson RL, Lancelot Y, et al (eds) Proceedings of the Ocean Drilling program, Scientific Results, vol 129

Ambrosio F (2020) A new statistical approach to the geochemical systematics of Italian alkaline igneous rocks. Open Geosci 12:133–147

Avanzinelli R, Sapienza GT, Conticelli S (2012) The Cretaceous to Paleogene within-plate magmatism of Pachino-Capo Passero (southeastern Sicily) and Adria (La Queglia and Pietre Nere, southern Italy): geochemical and isotopic evidence against a plume-related origin of circum-Mediterranean magmas. Eur J Mineral 24(1):73–96

Barbieri M, Ferrini V (1984) Il rapporto 87Sr/86Sr nella ipoabissalite di Pescosansonesco (PE). Ren Soc It Miner Petrol 39:497–501

Barbieri M, Ghiara MR, Stanzione D, Villar LM, Pezzutti NE, Segal SJ (1997) Trace-element and isotope constrains on the origin of ultramafic lamproprhyres from Los Alisos (Sierra Subandinas Northern Argentina). J S Amer Earth Sci 10:39–47

Bell K, Lavecchia G, Rosatelli G (2013) Cenozoic Italian magmatism – Isotope constraints for possible plume-related activity. J S Am Earth Sci 41:22–40

Bellini E (1957) Segnalazione di una roccia serpentinosa nell'Appennino Pescarese. Boll Serv Geol D'Italia, LXXIX:745–747

Bello S, Scott CP, Ferrarini F, Brozzetti F, Scott T, Cirillo D, de Nardis R, Arrowsmith RJ, Lavecchia G (2021) High-resolution surface

faulting from the 1983 Idaho Lost River Fault Mw 6.9 earthquake and previous events. Sci Data 8(68):1–20
Bello S, Andrenacci C, Cirillo D, Scott CP, Brozzetti F, Arrowsmith RJ, Lavecchia G (2022) High-detail fault segmentation: Deep insight into the anatomy of the 1983 Borah Peak earthquake rupture zone (Mw 6.9, Idaho, USA). Lithosphere 2022(1):8100224
Bemis SP, Micklethwaite S, Turner D, James MR, Akciz S, Thiele ST, Bangash HA (2014) Ground-based and UAV-Based photogrammetry: A multi-scale, high-resolution mapping tool for structural geology and paleoseismology. J Struct Geol 69:163–178
Bigi S, Calamita F, Centamore E (1995) Caratteristiche geologico-strutturali dell'area abruzzese ad oriente del Gran Sasso. Stud Geol Camerti 2:67–76
Bigi S, Di Bucci D (1987) Rilevamento geologico delle strutture di Mt Picca e di Mt La Queglia, Appennino Abruzzese. Geol Romana 26:413–418
Broom-Fendley S, Styles MT, Appleton DA, Gunn AG, Wall F (2016) Evidence for dissolution-reprecipitation of apatite and preferential LREE mobility in carbonatite-derived late-stage hydrothermal processes. Am Miner 101:596–611
Brozzetti F, Cerritelli F, Cirillo D, Agostini S, Lavecchia G (2020) The roccacaramanico conglomerate (Maiella Tectonic Unit) in the frame of the Abruzzo early pliocene foreland basin system: Stratigraphic and structural implications. Ital J Geosci 139(2):266–286
Chalapati Rao NV, Dharma Rao CV, Das S (2012) Petrogenesis of lamprophyres from Chhota Udepur area, Narmada rift zone, and its relation to Deccan magmatism. J Asian Earth Sci 45:24–39
Chakhmouradian AR, Reguir EP, Kamenetsky VS, Sharygin VV, Golovin AV (2013) Trace-element partitioning in perovskite: Implications for the geochemistry of kimberlites and other mantle-derived undersaturated rocks. Chem Geol 353:112–131
Cirillo D (2020) Digital Field Mapping and Drone-Aided Survey for Structural Geological Data Collection and Seismic Hazard Assessment: Case of the 2016 Central Italy Earthquakes. Appl Sciences 10:5233
Cirillo D, Cerritelli F, Agostini S, Bello S, Lavecchia G, Brozzetti F (2022) Integrating Post-Processing Kinematic (PPK)–Structure-from-Motion (SfM) with Unmanned Aerial Vehicle (UAV) Photogrammetry and Digital field mapping for structural geological analysis. ISPRS Int J Geo-Inf 11:437
Coulson IM, Goodenough KM, Pearce NJM, Leng MJ (2003) Carbonatites and lamprophyres of the Gardar Province – a 'window' to the sub-Gardar mantle? Mineral Mag 67(5):855–872
Cundari A, Ferguson AK (1982) Significance of the pyroxene chemistry from leucite-bearing and related assemblages. Tschermaks Min Petr Mitt 30:189–204
Deer WA, Howie RA, Zussman J (1997) Rock forming minerals. The Geological Society, London
Delor CP, Rock NMS (1991) Alkaline-ultramafic lamprophyre dykes from the Vestfold Hills, Princess Elizabeth Land (East Antarctica): primitive magmas of deep mantle origin. Antarct Sci 3(4):419–432
Doroshkevich AG, Chebotarev DA, Sharygin VV, Prokopyev IR, Nikolenko AM (2019) Petrology of alkaline silicate rocks and carbonatites of the Chuktukon massif, Chadobets upland, Russia: Sources, evolution and relation to the Triassic Siberian LIP. Lithos 332–333:245–260
Durazzo A, Taylor LA, Shervais JW (1984) Ultramafic Lamprophyre in a Carbonate Platform Environment, Mt. Queglia, Abruzzo. Italy Neues Jahrbuch Miner Abh 150:199–217
Edgar AD (1989) Barium- and strontium-enriched apatites in lamproites from West Kimberley. Western Australia Am Mineral 74(7–8):889–895
Ghisetti F, Vezzani L (1991) Thrust belt development in the central Apennines (Italy): Northward polarity of thrusting and out-of-sequence deformations in the Gran Sasso Chain. Tectonics 10(5):904–919
Goto A, Fujimaki H, Morikiyo T, Liu J (2004) Finding dolomitic melnoite diatreme at Badou in the Laiwu-Zibo area, Shandong province, China. Proc Jpn Acad, Ser B 80(6):269–275
Graham S, Lambert DD, Shee SR, Pearson NJ (2002) Juvenile lithospheric mantle enrichment and the formation of alkaline ultramafic magma sources: Re-Os, Lu-Hf and Sm-Nd isotopic systematics of the Norseman melnoites. Western Australia Chem Geol 186(3–4):215–233
Graham S, Lambert D, Shee S (2004) The petrogenesis of carbonatite, melnoite and kimberlite from the Eastern Goldfields Province. Lithos 79(1–4):519–533
He Q, Xiao L, Balta B, Gao R, Chen J (2010) Variety and complexity of the Late-Permian Emeishan basalts: Reappraisal of plume-lithosphere interaction processes. Lithos 119:91–107
Hoch M (1999) Geochemistry and petrology of ultramafic lamprophyres from Schirmacher Oasis. East Antarctica Mineral Petrol 65:51–67
James MR, Robson S (2012) Straightforward reconstruction of 3d surfaces and topography with a camera: Accuracy and geoscience application. J Geophys Res Earth Surf 117:17
Kapustin YL (1977) Distribution of Sr, Ba, and the rare earths in apatite from carbonatite complexes. Geochem Int 14(4):71–80
Kargin AV, Golubeva YY, Demonterova EI, Koval'chuk EV (2017) Petrographic-Geochemical Types of Triassic Alkaline Ultramafic Rocks in the Northern Anabar Province, Yakutia. Russia Petrol 25(6):535–565
Kogarko LN, Ryabchikov ID, Kuzmin DV (2012) High-Ba mica in olivinites of the Guli massif (Maymecha-Kotuy province, Siberia). Russ Geol 53(11):1209–1215
Lavecchia G, Bell K (2012) Magmatectonic zonation of Italy: a tool to understanding Mediterranean geodynamics. In: Stoppa F (ed) Updates in volcanology: a comprehensive approach to volcanological problems. 2011. ISBN: 978-953-307-434-4
Lavecchia G, de Nardis R, Ferrarini F, Cirillo D, Bello S, Brozzetti F (2021) Regional Seismotectonic Zonation of Hydrocarbon Fields in Active Thrust Belts: A case study from Italy. In: Bonali FL, Pasquaré Mariotto F, Tsereteli N (eds) Building Knowledge for Geohazard Assessment and Management in the Caucasus and other Orogenic Regions. NATO Science for Peace and Security Series C: Environmental Security. Springer, Dordrecht
Lavecchia G, Bello S, Andrenacci C, Cirillo D, Ferrarini F, Vicentini N, de Nardis R, Roberts G, Brozzetti F (2022) QUaternary fault strain INdicators database - QUIN 1.0 - first release from the Apennines of central Italy. Sci Data 9(1)204:1–16
Le Maitre RE (2002) Igneous Rocks: A classification and Glossary of Terms, 2nd edn. Cambridge University Press, Cambridge, p 236
Le Roex AP, Lanyon R (1998) Isotope and trace element geochemistry of Cretaceous Damaraland lamprophyres and carbonatites, Northwestern Namibia: evidence for plume-litosphere interactions. J Petrol 39(6):1117–1146
Liu Y, Hou ZQ (2017) A synthesis of mineralization styles with an integrated genetic model of carbonatite-syenite-hosted REE deposits in the Cenozoic Mianning-Dechang REE metallogenic belt, the eastern Tibetan Plateau, southwestern China. J S Am Earth Sci 137:35–79
Liu Y, Chakhmouradian AR, Hou ZQ, Song WL, Kynicky J (2018) Development of REE mineralization in the giant Mouniuping deposit (Sichuan, China): insights from mineralogy, fluid inclusions, and trace-element geochemistry. Miner Deposita 54:701–718
Malpas H, Foley SF, King AF (1986) Alkaline mafic and ultramafic lamprophyres from the Aillik Bay area, Labrador. Can J Earth Sci 23:1902–1918
Mitchell RH (1994) Suggestions for the revisions to the terminology of kimberlites and lamprophyres from a genetic viewpoint. In: Meyer HOA, Leonardos OH (eds) Kimberlites, Related Rocks

and Mantle Xenoliths. Proc Fifth Internat Kimberlite Conf, vol 1. Araxá, Brazil, June 1991, pp 15–26
Mitchell RH (1995) Kimberlites, orangeites and related rocks. Plenum Press, New York, p 410
Mitchell RH (2009) Peralkaline nephelinite–natrocarbonatite immiscibility and carbonatite assimilation at Oldoinyo Lengai. Tanzania Contrib Mineral Petrol 158:589
Pandey R, Chalapathi Rao NV, Dhote P, Pandit D, Choudhary AK, Sahoo S, Lehmann B (2017) Rift-associated ultramafic lamprophyre (damjernite) from the middle part of the Lower Cretaceous (125 Ma) succession of Kutch, northwestern India: Tectonomagmatic implications. Geosci Front 9(6):1883–1902
Panina LI, Stoppa F, Usol'tseva LM (2003) Genesis of melilitite rocks of Pian di Celle Volcano, Umbrian Kamafugite Province, Italy: Evidence from melt inclusions in minerals. Petrology 11(4):365–382
Pearce JA (2008) Geochemical fingerprinting of oceanic basalts with applications to ophiolite classification and the search for Archean oceanic crust. Lithos 100:14–48
Prelevic D, Akal C, Romer RL, Mertz-Kraus R, Helavci C (2015) Magmatic response to slab tearing: constraints from the Afyon Alkaline Volcanic Complex. Western Turkey J Petrol 56(3):527–562
Reguir EP, Chakmouradian AR, Pisiak L, Haden NM, Yang P, Xu C, Kynicky J, Coueslan CG (2012) Trace-element composition and zoning in clinopyroxene- and amphibole-groupminerals: Implications for element partitioning and evolution of carbonatites. Lithos 128–131:27–45
Rileya TR, Leata PT, Storeyb BC, Parkinsonc IJ, Millar IL (2003) Ultramafic lamprophyres of the Ferrar large igneous province: evidence for the HIMU mantle component. Lithos 66:63–76
Rock NMS (1986) The nature and origin of Ultramafic Lamprophyres: Alnöites and Allied Rocks. J Petrol 27(1):155–196
Rock NMS (1991) Lamprophyres. Blackie and Son Ltd, p 285
Rosatelli G, Wall F, Le Bas MJ (2003) Potassic glass and calcite carbonatite in lapilli from extrusive carbonatites at Rangwa Caldera Complex. Kenya Mineralogical Magazine 66(5):931–955
Rosatelli G, Wall F, Stoppa F (2007) Calcio-carbonatite melts and metasomatism in the mantle beneath Mt. Vulture (Southern Italy). Lithos 99(3–4):229–248
Scisciani V, Bigi S, Calamita F (2000) Shortcut geometry along the N-S trending Gran Sasso and Morrone thrust front (Central Apennines). Mem Soc Geol It 55:175–183
Stoppa F, Liu Y (1995) Chemical composition and petrogenetic implications of apatites from some ultra-alkaline Italian rocks. Eur J Miner 7:391–402
Stoppa F, Cundari A (1998) Origin and multiple crystallization of the kamafugite-carbonatite association: the San Venanzo-Pian di Celle occurrence (Umbria, Italy). Mineral Mag 62(2):273–289
Stoppa F, Woolley AR, Cundari A (2002) Extension of the melilite-carbonatite province in the Appennines of Italy: the kamafugite of Grotta del cervo. Abruzzo Mineral Mag 66(4):555–574
Stoppa F, Cundari A, Rosatelli G, Woolley AR (2003) Leucite melilitolites in Italy: genetic aspects and relationships with associated alkaline rocks and carbonatites. Per Mineral, Spec issue, Eurocarb, pp 223–251
Stoppa F (2008) Italian carbonatites and the mechanism of Earth CO2 discharge. Geochim Cosmochim Acta 72(12):A904
Stoppa F, Rukhlov AS, Bell K, Schiazza M, Vichi G (2014) Lamprophyres of Italy: early Cretaceous alkaline lamprophyres of Southern Tuscany, Italy. Lithos 188:97–112
Stoppa F, Pirajno F, Schiazza M, Vladykin NK (2016) State of the art: Italian carbonatites and their potential for critical-metal deposits. Gondwana Res 37:152–171
Stoppa F, Schiazza M, Rosatelli G, Castorina F, Sharygin VV, Ambrosio FA, Vicentini N (2019) Italian carbonatite system: from mantle to ore-deposit. Ore Geol Rev 114:103041
Stoppa F (2021) Evolution and involution of carbonatite thoughts. In: Yaxley GM, Anenburg M, Timmerman S (eds) Carbonatites. Elements 17(5):303–304
Sun SS, McDonough WF (1989) Chemical and isotopic systematics of oceanic basalts: implications for mantle composition and processes. Geol Soc Spec Publ 42:313–345
Tappe S, Jenner GA, Foley SF, Heaman L, Besserer D, Kjarsgaard BA, Ryan B (2004) Torngat ultramafic lamprophyres and their relation to the North Atlantic Alkaline Province. Lithos 76:491–518
Tappe S, Foley SF, Jenner GA, Kjarsgaard BA (2005) Integrating Ultramafic Lamprophyres into the IUGS classification of Igneous Rocks: rationale and implications. J Petrol 46(9):1893–1900
Tappe S, Foley SF, Jenner GA, Heaman LM, Kjarsgaard BA, Romer RL, Stracke A, Joyce N, Hoefs J (2006) Genesis of ultramafic lamprophyres and carbonatites at Aillik Bay, Labrador: a consequence of incipient lithospheric thinning beneath the North Atlantic craton. J Petrol 47:1261–1315
Taylor SR, McLennan SM (1985) The continental crust: its composition and evolution. Blackwell Scientific Publications, Oxford, p 312
Ulrych J, Dostal J, Hegner E, Balogh K, Ackerman L (2008) Late Cretaceous to Paleocene melilitic rocks of the Ohře/Eger Rift in northern Bohemia, Czech Republic: Insights into the initial stages of continental rifting. Lithos 101:141–161
Ulrych J, Adamovič J, Krmíček L, Ackerman L, Balogh K (2014) Revision of Scheumann's classification of melilitic lamprophyres and related melilitic rocks in light of new analytical data. J Geosci 59(1):3–22
Upton BGJ, Emeleus CH, Heaman LM, Goodenough KM, Finch AA (2003) Magmatism of the mid-Proterozoic Gardar Province, South Greenland: chronology, petrogenesis and geological setting. Lithos 68(1–2):43–65
Vichi G, Stoppa F, Wall F (2005) The carbonate fraction in carbonatitic Italian lamprophyres. Lithos 85(1–4):154–170
Vuorinen JH, Hafi Lenius U, Whitehouse MJ, Mansfeld J, Skelton ADL (2005) Compositional variations (major and trace elements) of clinopyroxene and Ti-andradite from pyroxenite, ijolite and nepheline syenite, Alnö Island, Sweden. Lithos 81:55–77
Wanke H, Dreidus G, Jagoutz E (1984) Mantle chemistry and accretion history of the Earth. Archean Geochemistry 1–24
Westoby MJ, Brasington J, Glasser NF, Hambrey MJ, Reynolds JM (2012) 'Structure-from-motion' photogrammetry: A low-cost, effective tool for geoscience applications. Geomorphology 179:300–314
Woolley AR, Bailey K, Castorina F, Rosatelli G, Stoppa F, Wall F (2005) Reply to: "Carbonate-rich pyroclastic rocks from central Apennines: Carbonatites or carbonated rocks? A commentary". A Peccerillo Periodico Di Mineralogia 74(3):183–194
Wyllie P, Huang, W-L (1975) Influence of mantle CO_2 in the generation of carbonatites and kimberlites. Nature 257(5524):297–299
Zaccaria D, Vicentini N, Perna MG, Rosatelli G, Sharygin VV, Humphreys-Williams E, Brownscombe W, Stoppa F (2021) Lamprophyre as the source of zircon in the Veneto Region. Italy Minerals 11(10):1081
Zappettini EO, Villar LM, Hernandez LB (2015) Mineral chemistry and petrogenesis of the Puesto La Peña undersaturated alkaline potassic complex, Mendoza, Argentina. Can Mineral 53:717–756
Zhang RY, Liou JG (2003) Clinopyroxenite from the Sulu ultrahigh-pressure terrane, eastern China: Origin and evolution of garnet exsolution in clinopyroxene. Am Mineral 88(10):1591–1600
Zozulya DR, Kullerud K, Ribacki E, Altenberger U, Sudo M, Savchenko YE (2020) The newly discovered Neoproterozoic aillikite occurrence in Vinoren (Southern Norway): age, geodynamic position and mineralogical evidence of diamond-bearing mantle source. Minerals 10:1029

Authors and Affiliations

Giada Vichi[1] · Maria Grazia Perna[1,2] · Francesco Ambrosio[1] · Gianluigi Rosatelli[1,2] · Daniele Cirillo[1,3] · Sam Broom-Fendley[4] · Nikolay V. Vladykin[5] · Daria Zaccaria[1,2] · Francesco Stoppa[1,2]

1 DiSPuTer, Università G. d'Annunzio, Via dei Vestini, 31, 66100 Chieti, Italy

2 CAST, Center for Advanced Studies and Technology, Università G. d'Annunzio, Via dei Vestini, 31, 66100 Chieti, Italy

3 CRUST - Centro inteRUniversitario per l'analisi Sismotettonica Tridimensionale, Chieti, Italy

4 Camborne School of Mines, University of Exeter, Penryn Campus, Cornwall TR10 9FE, UK

5 Vinogradov Institute of Geochemistry, SBRAS, 1a Favorsky St, Irkutsk 664033, Russia